Knudsen diffusion in beds of monodisperse silica spheres
by David Gary Huizenga

A thesis submitted in partial fulfillment of the requirements for the degree of Master of Science in Chemical Engineering
Montana State University

Abstract:
The accurate prediction of effective Knudsen diffusivities in porous media has become increasingly important to the chemical engineer. In an attempt to shed insight into this problem, a model porous pellet of known geometry was constructed by randomly packing together uniform submicron silica spheres. Monodisperse sets of spheres were produced with an average sphere radius range from 52 to 305 nm. By using sets of spheres with a different average radius, the average pore radius in the model porous pellet could be manipulated. The average porosity of the pellets, 0.36 ± 0.03, coincided with literature values for a random packing of spheres. The porosity was found to be quite independent of sphere size and packing pressure in the packing pressure range from 1,000 to 10,000 psi.

A “plug flow” apparatus was constructed to measure the diffusivity through a single pellet. The Knudsen diffusivities of a number of low molecular weight gases were then investigated using a series of pellets with increasing average pore radius. This radius was defined using a hydraulic radius concept and was a function of sphere size and pellet porosity only. The tortuosity factor determined in the beds of spheres ranged from 1.45 to 1.5 L The tortuosity factor was identical for all gases investigated and was independent of sphere size within the error limits of the investigation.

KNUDSEN DIFFUSION IN BEDS OF MONODISPERSE SILICA SPHERES

by

David Gary Huizenga

A thesis submitted in partial fulfillment
of the requirements for the degree

of

Master of Science

in

Chemical Engineering

MONTANA STATE UNIVERSITY
Bozeman, Montana

August 1984

APPROVAL

of a thesis submitted by

David Gary Huizenga

This thesis has been read by each member of the thesis committee and has been found to be satisfactory regarding content, English usage, format, citation, bibliographic style, and consistency, and is ready for submission to the College of Graduate Studies.

8/3/84
Date

Douglas Smith
Chairperson, Graduate Committee

Approved for the Major Department

Aug 3, 1984
Date

John T. Sears
Head, Major Department

Approved for the College of Graduate Studies

8-6-84
Date

M R Malone
Graduate Dean

STATEMENT OF PERMISSION TO USE

In presenting this thesis in partial fulfillment of the requirements for a master's degree at Montana State University, I agree that the Library shall make it available to borrowers under rules of the Library. Brief quotations from this thesis are allowable without special permission, provided that accurate acknowledgment of source is made.

Permission for extensive quotation from or reproduction of this thesis may be granted by my major professor, or in his absence, by the Dean of Libraries when, in the opinion of either, the proposed use of the material is for scholarly purposes. Any copying or use of the material in this thesis for financial gain shall not be allowed without my permission.

Signature David S Hungerford

Date 8/3/84

ACKNOWLEDGMENTS

The author would like to thank the faculty and staff of the Chemical Engineering Department at Montana State University for their help and guidance. The insight and encouragement given by my advisor, Dr. Douglas M. Smith, is greatly appreciated. Special thanks is also extended to my coworkers, Mark Drake and Mukesh Turakhia, for their assistance during various phases of this investigation. Finally, I would like to acknowledge the financial support received from Sigma Xi, the Scientific Research Foundation, by the Research Creativity Program established by Montana State University and from the Engineering Experiment Station at Montana State University.

TABLE OF CONTENTS

TABLE OF CONTENTS—Continued

LIST OF TABLES

LIST OF FIGURES

NOMENCLATURE

A	Cross sectional area of pellet
C_A	Concentration of Component A
C_1, C_2	Inlet and Outlet Concentrations, respectively
D	General Diffusion Coefficient
D_e	Effective Diffusivity
D_K	Knudsen Diffusivity
F	Molar Flow Rate of Gas
f	Sticking Coefficient
g	grams
L	Length of Pellet
MW	Molecular Weight
N_A	Flux of Component A
P	Gas Pressure
P_o	Saturation Pressure of Gas
P_m	External Applied Pressure (mercury porisimetry)
R	Gas Constant
r	Pore Radius
$\bar{r}$	Mean Pore Radius
r_h	Hydraulic Radius
r_s	Sphere Radius
SA	Surface Area (per gram of solid)
s	Seconds

T	Temperature
V_P	Total Pore Volume (per gram of solid)
V_L	Molar Volume (liquid)
$V_{P_{el}}$	Total Pellet Volume
δ	Thickness of Adsorbed Molecular Layer
ϵ	Porosity, Void Fraction
λ	Mean Free Path
ρ_s	True Density of Solid Spheres
σ	Surface Tension
τ	Tortuosity Factor
$\overline{\nu}$	Molecular Velocity

ABSTRACT

The accurate prediction of effective Knudsen diffusivities in porous media has become increasingly important to the chemical engineer. In an attempt to shed insight into this problem, a model porous pellet of known geometry was constructed by randomly packing together uniform submicron silica spheres. Monodisperse sets of spheres were produced with an average sphere radius range from 52 to 305 nm. By using sets of spheres with a different average radius, the average pore radius in the model porous pellet could be manipulated. The average porosity of the pellets, 0.36 ± 0.03, coincided with literature values for a random packing of spheres. The porosity was found to be quite independent of sphere size and packing pressure in the packing pressure range from 1,000 to 10,000 psi.

A "plug flow" apparatus was constructed to measure the diffusivity through a single pellet. The Knudsen diffusivities of a number of low molecular weight gases were then investigated using a series of pellets with increasing average pore radius. This radius was defined using a hydraulic radius concept and was a function of sphere size and pellet porosity only. The tortuosity factor determined in the beds of spheres ranged from 1.45 to 1.51. The tortuosity factor was identical for all gases investigated and was independent of sphere size within the error limits of the investigation.

INTRODUCTION AND LITERATURE REVIEW

The Problem-Predicting Tranport Rates in Porous Media

Diffusion in Porous Media

The transport of gases through porous media is of interest in a diverse range of fields including physics, physical chemistry, biology, geology and the engineering disciplines. Of particular interest to the chemical engineer, applications include catalysis, combustion, sorption, gas separations and nuclear waste isolation. For the correct design and utilization of any porous media an accurate prediction of the mass transfer rate is a necessity [1]. In many of the above applications gas molecules will be subjected to movement through relatively small pores and/or at relatively low pressures. Under these conditions one or more forms of diffusional transport will predominate, in contrast to bulk flow movement.

Weisz [2] has characterized the various diffusional mechanisms for gaseous transport in porous media as follows:

1. Bulk diffusion—Transport is governed by molecule-molecule collisions. The mean free path of the gas molecule in question is much less than the average pore radius ($r/\lambda > 10$) [3].
2. Knudsen diffusion—Transport is dominated by molecule-pore wall interactions ($r/\lambda < \frac{1}{10}$) [3].
3. Configurational diffusion—The mass transfer rate is governed by specific molecule-pore wall interactions due to the molecule and the diameter of the pore being of the same order of magnitude.
4. Surface diffusion—If the diffusing gas adsorbs, surface transport of adsorbed molecules may facilitate the overall migration rate.

To employ one or more of the above mechanisms necessitates the use of Fick's First Law [1]:

$$N_A = - D \frac{dC_A}{dx} \tag{1}$$

The flux of component A, N_A, is relative to stationary coordinates and is seen to be proportional to the concentration gradient of compound A in the direction of flow. The proportionality constant, D, will vary in magnitude depending on the predominating mechanism for diffusional transport.

This investigation will be centered on the transport rate observed when the primary movement of molecules is due to diffusion in the Knudsen regime. Understanding transport in this regime has become increasingly more important due to the attractiveness of operating systems at lowered pressures, thereby eliminating the cost of high pressure vessels, and also because of the economic benefits associated with designing new chemical synthesis based on heterogeneous catalysis. The chemical and petroleum industries are investing large sums in this development of more efficient porous solid catalysts [1]. The most effective use of these supports depends, in large part, on predicting mass transfer rates in and out of a porous pellet. The desire to increase reaction surface area in the pellets often produces transport in the Knudsen regime.

In this regime the characteristic pore size is often much smaller than λ, and the migrating gas molecules are much more likely to intersect the pore wall in contrast to interacting with other gas molecules. It is postulated that the molecules hit the walls and are momentarily adsorbed, subsequently to be given off in random directions. Therefore, it is reasonable to assume that the Knudsen diffusivity, D_K, depends on the magnitude of both the molecular velocity, $\bar{v}$, and the pore radius, r. Indeed, simple kinetic theory describes the Knudsen diffusivity as [4]:

$$D_K = \frac{2}{3} r \bar{v} \tag{2}$$

For diffusion in capillaries at low pressures Knudsen has derived the following expression for D_K [5]:

$$D_K = \frac{4}{3} r \sqrt{\frac{2RT}{\pi MW}} \left(\frac{2 - f}{f} \right) \tag{3}$$

where f = fraction of molecules which stick to the pore wall

MW = molecular weight

R = gas constant

T = temperature

For most practical applications the sticking coefficient, f, was found to be unity and Eq. 3 reduces to the working equation in cgs units [4]:

$$D_K = 9700 r \sqrt{\frac{T}{MW}} \tag{4}$$

where D_K is in cm^2/s, r is in cm and T is in °C.

Modelling Porous Media

We now have a means for predicting the Knudsen diffusivity of gases for the ideal case of straight uniform cylindrical pores. Few, if any, real porous media can accurately be thought of as consisting of a bundle of parallel pores without some modification. Because of the complexity of the geometry of the void spaces in real porous media a model must be assumed. Optimally, the model would include a realistic representation of the pore structure with acceptable mathematics and be described by easily determined physical parameters. Traditionally the models have been linked to the total surface area, SA, and total pore volume, V_P, per gram of solid, the average pore radius, $\bar{r}$, and the pore volume distribution.

Wheeler [6] proposed the simple Parallel-pore Model based on a mean pore radius defined as:

$$\bar{r} = \frac{2V_P}{SA} \tag{5}$$

To make use of $\bar{r}$, Wheeler replaced a complex porous pellet with an assembly of cylindrical pores of porosity, ϵ, and all with radius $\bar{r}$. The true path length of diffusion is the remaining unknown necessary to calculate an effective diffusivity, D_e, for the model porous media. This length would be a function of the actual orientation of the pores, relative to each other, and the non-uniformity of the actual pore radii. Because this length cannot be predicted from first principles, an adjustable parameter, the tortuosity τ, is introduced to complete the definition of the effective diffusivity:

$$D_e = \frac{D_K \epsilon}{\tau} \tag{6}$$

Eq. 1 may now be modified for use with porous media:

$$N_A = - \frac{D_K \epsilon}{\tau} \frac{dC_A}{dx} \tag{7}$$

A great deal of work has been done in an attempt to generalize values of τ coincident with the various physical parameters of the porous media. Values vary from 1 to 8, with a generally accepted value of 3 for systems of long cylindrical pores [7,8]. In the absence of pertinent information regarding the value of the tortuosity factor a value of $1/\epsilon$ has often been used [1].

In an attempt to more accurately model porous media characterized by wide pore size distributions several other more complicated models have been proposed. Johnson and Stewart [8] proposed the Parallel-Path pore Model. This model pictures the voids as an array of parallel cylinders and pores and incorporates an experimentally determined pore volume distribution. Wakao and Smith [10] envisioned a bidisperse porous media described

by regions of micro and macro porosity. It now becomes necessary to specify the micro and macro effective diffusivities and relate the quantity of gas in the micropores to that in the macropores at equilibrium. A similar model has been proposed by Ruckenstein et al. [11] for transient uptake. Finally, a number of general models have been proposed which include all mechanisms of transport in the porous media. The resulting mathematics and uncertainties involved in parameter estimation render these models too complex for most applications, however.

An Agglomerated Sphere Model

One is understandably drawn to Wheeler's parallel pore model for its conceptual and mathematical simplicity. Unfortunately, as previously indicated, it is difficult to justify characterizing the majority of commercially available porous media as bundles of uniform cylinders. In particular, the pore structure of many solids more often resembles the void volume contained in a random assemblage of solid spheres [12]. The pelleting or extruding of fine alumina or silica sols in the catalyst industry is a typical representation of such a porous media [1].

The modelling of porous media as an assemblage of spheres could be interpreted as representing the opposite limiting case to the parallel pore model. It is the desire of this work to use the simple form of Eq. 7 to accurately predict the flux through a bed of monodisperse spheres. The obvious question begging address is the assignment of meaningful values for the average pore radius and the tortuosity factor. It therefore becomes necessary to examine the traditional measurement techniques and decide on the best convention by which to realistically assign a value for $\bar{r}$ in a bed of randomly packed uniform spheres. Having decided on a value for $\bar{r}$ would subsequently yield a value for the tortuosity factor for this complex but realistic geometry.

The average pore radius is commonly obtained by using mercury porisimetry techniques, analysis of sorption isotherms or by incorporating the ratio of the total pore volume to the total surface area.

Mercury porisimetry measurements are based on mercury's high surface tension, σ, and its tendency not to wet most solid surfaces. Basically, an external pressure is applied to a known volume of mercury forcing it into the pores of the sample material. The change in remaining volume of mercury with increasing pressure is recorded. Ritter and Drake quantified the process by equating the force due to surface tension to the applied force. Assuming cylindrical pores they obtained [13]:

$$\pi r^2 P_m = - 2\pi r \sigma \cos\theta \tag{8}$$

where θ is the contact angle between the mercury and the pore wall and is usually taken to be a constant 140°, P_m is the external applied pressure and σ is the surface tension. With a high pressure mercury porisimeter (60,000 psia) pore radii from 2 nm to 1000 nm can be measured. From plots of the cumulative pore volume versus the pore radius the average pore radius is determined [14].

A second method utilizes sorption isotherm data to determine pore radii. As adsorption experiments are continued to saturation pressures, condensation in the pores of the sample becomes complete. The pore volume distribution can now be calculated by employing the Kelvin equation, as it gives the relationship between the equilibrium vapor pressure and the concave surface of the meniscus in the pores. With a correction for the adsorbed molecules on the pore walls the Kelvin equation predicts pore radii of cylindrical pores as follows [4]:

$$r - \delta = - \frac{2\sigma V_L \cos\theta}{RT \ln (P/P_0)} \tag{9}$$

where δ is the thickness of the adsorbed layers, V_L is the molar volume of condensed liquid and $\theta = 0$ is the contact angle at the pore wall. Due to questionable assumptions when

using the Kelvin equation with very small pores and over-sensitivities involved with measuring large pores, the sorption technique is limited to a reliable pore radii range of 1 nm to 20 nm. As with mercury porisimetry techniques, a plot of cumulative volume displaced versus pore radii will yield the average pore radius.

Choosing the Proper Average Pore Radius

It is important to note that both of the commonly used methods detailed above model the pore structure as a collection of cylinders. We know intuitively that this cannot be the case for an agglomeration of spheres. Brunauer et al. [15] developed a means to determine pore volume distributions wherein the pore shape has little influence. The mathematics quickly becomes complicated, but the outcome results in the use of a hydraulic radius concept much the same as Wheeler postulated [14]. The hydraulic radius is defined as:

$$r_h = \frac{V_P}{SA} \tag{10}$$

where V_P and SA are defined as in Wheeler's model. For cylinders and parallel flat plates r_h is one half the radius or the distance between the plates. Brunauer first employed the use of a corrected r_h in models assuming cylindrical and flat plate geometries. However, working with a "modelless" uncorrected r_h, Brunauer ultimately showed that little error was produced in the pore volume analysis even for geometries differing greatly from the cylindrical or plate geometries. Smith [4] notes, however, that this "modelless" approach produces the most accurate values when the pore structure is relatively monodisperse and the surface area is high enough to be accurately determined, the surface area usually being determined by the Standard BET procedure [18].

Brunauer's method can produce values of pore radii a factor of two different from those obtained by mercury porisimetry/sorption analysis techniques. The meaning of the values obtained using the last two methods are in serious question, however, because they

represent the smallest cross section in a non-uniform pore [14]. In contrast, the use of the hydraulic radius concept, and therefore a radius predicted by Eq. 5, represents what might be considered to be a "true" average pore radius. In beds of uniformily sized spheres Eq. 5 may be reduced to a function of sphere radius and porosity only [17,18]

$$\bar{r} = 2 \frac{\frac{4}{3} \pi r_s^3}{4 \pi r_s^2} \left(\frac{\epsilon}{1 - \epsilon} \right) = \frac{2}{3} r_s \left(\frac{\epsilon}{1 - \epsilon} \right) \tag{11}$$

Thus an average pore radius has emerged which is a function of two easily determined physical parameters, and is also physically justified, in that it is not based on a cylindrical pore model. The radius for Eq. 11 could now be incorporated in calculating a flux using Eq. 7, the only unknown remaining being the tortuosity factor. If a monodisperse bed of spheres of known porosity comprised of spheres of known radii were available, and if the flux through the model porous media were measurable, the tortuosity factor could accurately be determined.

A Method for Investigation of Transport Rates in Model Porous Media

General Procedure

By relating the tortuosity factor to the average sphere size and porosity in a bed of uniform spheres, insight will be provided concerning transport in more realistic porous media, which are comprised of particles with a wider size distribution. Initially, however, it is prudent to minimize complications in the interpretation of results due to biases introduced by parameters of size and shape distributions [19]. The approach is, therefore, threefold in nature:

1. A monodisperse set of spheres in the proper size range with suitable physical and chemical properties must be produced.
2. The spheres must be randomly packed into pellets with realistic physical parameters (i.e., porosity and average pore radius).

3. An apparatus must be constructed to accurately measure the flux through this model porous media.

Uniform Spheres

The use of Eq. 11 for the calculation of an average pore radius necessitates the production of a monodisperse set of spheres. Mason [20] theoretically calculated that, for beds of randomly packed spheres ($\epsilon = 0.37$), porosimetry techniques would yield an average pore radius of 0.275 r_s. Assuming values of λ around 100 nm for typical gases at room temperature and 1 atm. pressure and using Mason's theorized pore radius, it is apparent that use of spheres in the colloidal size range will be necessary to insure a Knudsen diffusion mechanism.

A literature search reveals that there are several organic and inorganic materials which can be prepared as uniform spheres in the size range of interest. Those reported include polymer lattices [21] and particles of elemental selenium [22], chromium hydroxide [23], aluminum hydroxide [24], titania [25] and silica [19]. Silica particles were chosen for this investigation, the primary reasons being (1) they would fulfill the mechanical and thermal stability requirements, (2) silica is inert to a variety of solvents should this work be extended to liquid diffusion studies, and (3) the surface chemistry of silica has been widely investigated [26,27].

It is known that amorphous silica can be produced by the reaction of the tetra-esters of silica acid (tetra-alkyl silicates) with water. This reaction has many important commercial applications, including use in the binding of refractory and coating materials, in weatherproofing porous surfaces, in binding resins to glass and in the production of silica gel for catalysis and adsorption [28]. Due to the immiscibility of water and all alkyl silicates, the reaction must be carried out in a mutual solvent if homogenous conditions are to be maintained. The hydrolysis is catalyzed by acid or base solutions. Aelion et al. (29)

have studied the hydrolysis of tetra-ethyl orthosilicate (TEOS) under basic conditions and have suggested that the overall reaction takes place via two consecutive steps:

1. hydrolysis of ester to silicic acid

$$Si(OC_2H_5)_4 + 4H_2O \rightarrow Si(OH)_4 + 4C_2H_5OH \quad (12)$$

2. dehydration of silicic acid to form amorphous silica (particles or gel)

$$Si(OH)_4 \rightarrow \underline{SiO_2} + 2H_2O \quad (13)$$

Stöber et al. [19] discovered that, when the mutual solvent is an alcohol and ammonium hydroxide is used as a catalyst, the reaction between a number of short-chain tetra-alkyl silicates and water produces silica spheres having a very narrow size distribution under specifically controlled experimental conditions. By changing the alkyl group of either the mutual solvent or the alkyl silicate or by varying the concentrations of ammonia and/or water, they found that uniform particles could be reproducibly manufactured in a range of sizes from 0.05 to 2.0 μm. The size of the particles was determined using standard electron microscopic techniques.

Production of silica spheres in the lower size range will provide porous media with average pore radii of the appropriate magnitude for this study.

Construction of the Model Porous Pellet

Given a set of submicron uniform spheres, the formation and characterization of a model porous pellet is not yet reduced to a straightforward task. If the pellet is to be formed by pressing the spheres as a dry powder, Cadle et al. indicate care must be taken to insure an isotropic structure [30]. For the case of a random packing of spheres, isotropic would refer essentially to uniform porosity over the length of the pellets. Satterfield and Saraf [31] demonstrated that in pellets pressed from hard chromia-alumina catalyst powder, pellet heterogeneity could cause the local gas diffusivity to vary by a factor of as much as 2.5.

In an attempt to minimize contamination of the pore volume, lubricants and binders should be avoided. The excessive heats generated in the calcining processses (usually employed to remove these contaminants) might introduce undesirable sintering. In the absence of a binder relatively high pressures will be necessary to insure the integrity of the pellet in the flux measurement apparatus. However, care must be taken not to excessively compress the pellet and initiate fracturing of individual spheres.

The literature reveals bulk diffusional studies in beds of larger spheres, however, no information was found indicating measurement of pure Knudsen diffusivities in beds of submicron spheres. Hoogschagen [32] investigated bulk diffusion through beds of glass beads of porosities 0.35 to 0.43 and reported values of τ from 1.4 to 1.6. It is interesting to note that this range of porosities has been established as the inevitable outcome of randomly packing a bed of uniform spheres [33].

Haughey and Beveridge have reviewed the common regular packing schemes and various random packing models [17]. Although not really of practical application, it is interesting to note that the four common regular packings (1) rhombohedral (cubic close packed and face centered cubic), (2) tetragonal-sphenoidal, (3) orthorhombic, and (4) cubic have porosities of 0.26, 0.30, 0.40, and 0.48, respectively. It is of interest to note that for beds of uniform spheres the densest possible packing remains over one quarter void space.

One can also propose a variety of theoretical models for haphazardly or randomly positioning identical spheres in space. These models include Polyhedral [35], coupled sphere [36], local sphere shell [35], and the Monte Carlo model [12,35,38].

Just as each regular packing has a characteristic porosity, so also characteristic porosities can be attributed to various modes of randomly packed spheres. For example:

1. Very loose random packing—When a fluidized bed is slowly reduced from its minimum fluidization velocity it settles to an average porosity of 0.46 to 0.47 [39].

These values are similar to those obtained by the sedimentation of unimodal spheres [40].

2. Loose random packing—By dropping spheres into a container as a complete loose mass or by randomly hand packing, porosities of 0.40 to 0.41 are recorded [41]. Monte Carlo simulations generally produce values of ϵ in this range.
3. Poured random packing—Industrially packed beds are often continuously poured into the container with resulting porosities of 0.375 to 0.391 [42,43].
4. Close random packing—When beds of spheres are vigorously shaken or vibrated still lower values from 0.359 to 0.375 are observed [44-48].

The determination of the porosity of the model porous pellet can be achieved by several methods. One simple procedure involves boiling a weighed sample of pellets to displace the air in the voids with a liquid of known density. Dividing the increased weight by the density of the liquid yields the pore volume.

Gregg and Sing [47] detail the more accurate mercury-helium method. This method is based on helium's ability to completely penetrate the porous solid while mercury at low pressure is unable to move into the interior of the pellet. This method accurately gives values for the solid's true density and the porosity of the pellet.

If the density of the solid material is known and the volume of the pellet can be accurately measured. Eq. 14 may be used to calculate the porosity.

$$\epsilon = 1 - \frac{\text{wt. solid}}{\rho_s V_{P_{el}}} \tag{14}$$

where $V_{P_{el}}$ is the total volume of the pellet and ρ_s is the true density of the solid material.

Measuring Effective Diffusivities

Methods for determining effective diffusivities fall into two major categories, either steady-state or transient. In recent years a great deal of attention has been focused on the

development of the transient techniques in an attempt to compare these results with steady-state measurements. These comparisons can provide useful information about the internal pore structure (i.e., there could be dead end pores which were undetectable with steady-state methods).

Pulse-response methods are detailed by Haynes and Sarma [47], Drake [48], and Schneider and Smith [49]. These methods rely on analysis of response peaks from concentration pulses introduced into the material in question [50]. The response curves are fit to an appropriate mathematical model and a value of D_e is determined.

In that this investigation deals with solid spheres which should exhibit minimal microporosity, the effects due to dead end pore should be insignificant. This being true, the somewhat simpler steady-state methods may be employed. There are two basic steady-state methods—one employing the Wicke-Kallenbach diffusion cell [51], the other a "plug flow" apparatus.

The Wicke-Kallenbach or constant pressure, counter diffusion cell as it is sometimes referred to, allows two gases (i.e., hydrogen-nitrogen or helium-nitrogen) to flow past opposite sides of the porous sample such that no pressure gradient exists across the sample. The fluxes through the sample are calculated from a knowledge of the flow rates and concentrations of the two outlet streams [52]. This method can be used over a wide range of pressures and with some modification can also be employed over a moderate range of temperatures.

The "plug flow" apparatus operates under a constant pressure gradient and works best when Knudsen diffusion is the only mechanism for flow [1]. Typically, a "plug" of the porous material is positioned between two differing known concentrations of pure gas. By combination of the measured flow rate of gas through the plug with the known dimensions of the plug, a rearrangement of the integrated form of Fick's First Law, Eq. 15, will yield values of the effective diffusivity.

$$D_e = \frac{L}{A} \frac{F}{C_1 - C_2} \tag{15}$$

where $D_e = \frac{D_K \epsilon}{\tau}$

C_2 and C_1 = outlet and inlet concentrations, respectively

L = length of plug

A = cross sectional area of plug

F = flow rate of gas through plug

Research Objectives

It is the intent of this investigation to accurately predict mass transfer rates due to Knudsen diffusion in porous media. A model porous solid will be constructed of uniform submicron silica spheres. An attempt will be made to correlate the measured parameters of average sphere size and pellet porosity with an experimental diffusivity, thereby allowing calculation of the tortuosity factor.

MODEL POROUS MEDIA

Production of Uniform Silica Spheres

Reagents

The ethanol and methanol employed as solvents were of technical grade (98% pure). Water was house distilled prior to use. The tetraethyl and tetramethyl esters of silica acid were used as supplied in technical grade (Aldrich Chemical Co., Inc.). Ammonium hydroxide (14.9 M) was used as supplied in reagent grade. A constant concentration of ammonia was maintained throughout the investigation by initially fitting the bottle of ammonium hydroxide with a two-hole rubber stopper embracing a clamped dispensing outlet line and an inlet line. The inlet line was equipped with a bulb-type hand pump used to maintain a constant pressure above the solution.

Experimental Procedure

As determined by Stöber et al. [19] the concentrations of ammonia and water may be manipulated to produce colloidal suspensions of uniform spheres over a wide range of sizes. Their investigations also pointed out that varying the ester concentrations from 0.02 M to 0.5 M (other variables held constant) produced no significant change in particle size. An intermediate ester concentration of 0.28 M was used for all of the present experimentation.

In general, the desired volume of ammonium hydroxide and water were mixed with the appropriate amount of alcohol solvent in 250 ml Erlenmeyer flasks having ground glass stoppers. The water was added first and the ammonium hydroxide second. The stoppers were put in place immediately after pipeting the ammonium hydroxide, minimizing

loss of the volatile ammonia. The flasks were next mounted on an Eberbach shaker set to complete 60 back and forth movements per minute. The reactions took place at ambient temperatures (298-300 K). All batches were based on a final volume of 100 ml, therefore necessitating the addition of 6.4 ml of tetraethyl orthosilicate (TEOS) or 4.17 ml of tetramethyl orthosilicate (TMOS) to initiate the reaction. After an invisible hydrolytic reaction forming silicic acid (Equation 12), the condensation of the supersaturated silicic acid was indicated by an increasing opalescence of the mixture starting 1-5 minutes after the addition of the tetraalkyl silicate. Subsequently, the transition to a turbid white suspension occurred within a few more minutes.

As a standard procedure, samples for electron microscope investigation were taken 24 hours after the initiation of the reaction, although in most cases the particles had reached their final size at times sooner than this. All sampling for size determination was done by pipeting a drop of the suspension onto a formvar-coated copper T.E.M. (transmission electron microscope) grid. The grid was allowed to air dry, and subsequently electron micrographs of the particles retained on the grids were obtained using a JEOL 100-CX transmission and/or scanning electron microscope. The average particle size and standard deviation were determined with the aid of a Buehler Omnimet Image Analyzer. Typical sample sizes used in the characterization ranged from 200-400 particles.

The image analyzer was equipped with a television camera and a television screen and was used to enlarge the spherical particles to a size which could be accurately measured. The T.E.M. micrographs were printed to 20 X 25 cm black and white pictures for use on the image analyzer. The instrument was periodically calibrated with circles of known diameter. The projected diameters of the spheres, enlarged to approximately 30-60 mm, were then measured and recorded. From these measurements the average sphere diameter and standard deviation were calculated. Next the total number of spheres of a certain size were added together and this number was divided by the total number of particles measured. By doing this over the entire size range a histogram of sphere size distribution could be formed.

Results and Discussion

A typical TEM photograph (magnification = 76,000x) of spheres with average sphere diameter equal to 98 nm with a standard deviation of 8 nm is presented in Figure 1. The uniformity of both diameter and shape is readily apparent. This uniformity of sphere dimensions is further illustrated by Figure 2, a size distribution plot for the above batch of spheres. The spherical nature of the particles was consistent over a wide size range as can be seen by Figure 3, representing spheres of 650 nm diameter.

Standard deviations in particle diameters of 7 to 9% were typical over the entire size range of spheres produced. Stöber et al. reported values of 4 to 5% standard deviation in particle diameters [19]. It is thought that the tighter size distributions reported by Stöber were due to the use of more pure reagents. In particular, it appears that use of distilled tetra-alkyl silicates and Gold Seal grade alcohols would be necessary to achieve the narrower size distributions. However, for the present goal of constructing a model porous media the tighter size distribution was not considered necessary. That is to say, it was not thought that a 4% change in the size distribution would significantly effect the average pore size in the finished pellets.

Equation 11 was seen to relate the average pore size to the average sphere size. Therefore, one could vary the average pore radius by producing a variety of sets of uniform spheres over a range of radii. In the interest of reducing the number of experiments necessary to define the various concentrations of reactants which would yield particles of desired radii, an attempt was made to develop a suitable mathematical model to predict sphere size.

The experimental design was based on response surface methodology. This is a technique devoted to empirical modelling of relationships existing between a group of controlled experimental variables and the observed experimental results (i.e., sphere size) which serves as the dependent variable [53]. A systematic investigation of the influence

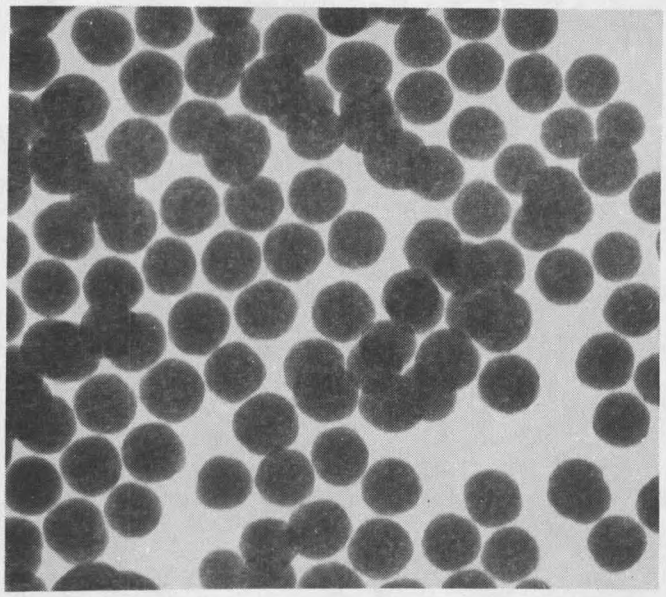

Figure 1. TEM micrograph of silica spheres (76,000x).

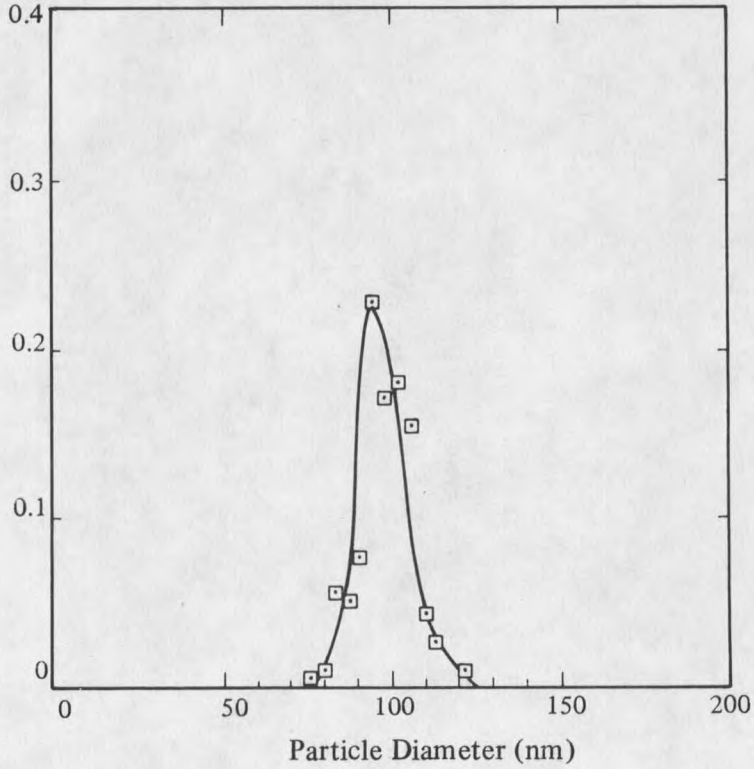

Figure 2. Typical silica sphere size distribution.

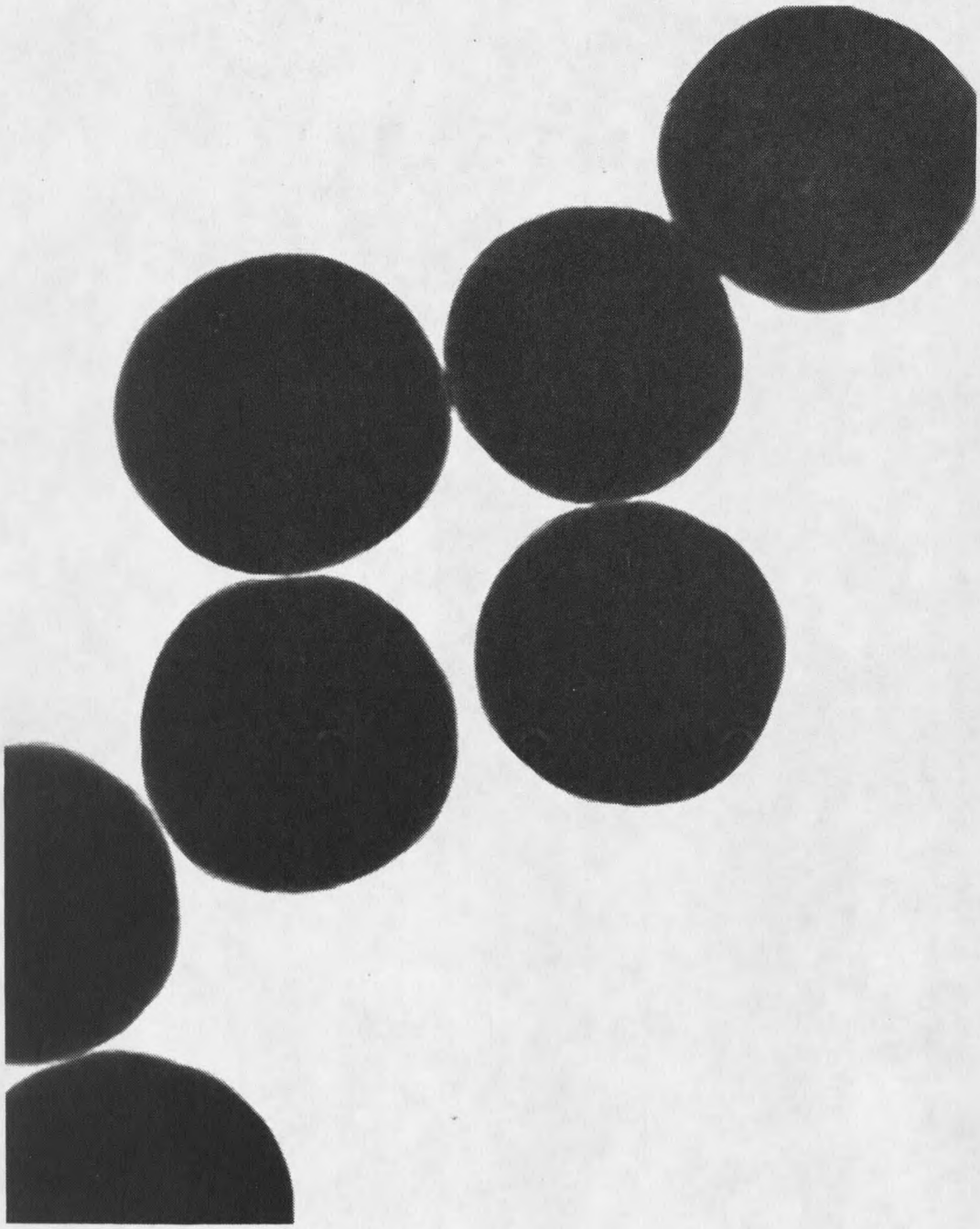

Figure 3. Observed spherical nature of 650 nm diameter particles.

of different water and ammonium hydroxide concentrations was made with the ethanol-TEOS system. The results are represented graphically in Figure 4 and Table 1, which is an analysis of variance table. Based on preliminary screening tests, a second order mathematical model was assumed to represent the response of sphere size to a change in the independent variables mentioned above. The large values of the F ratios revealed, however, that a higher order model would be necessary to describe the response. Briefly stated, the lack of fit F ratio indicates that the inability of the model to accurately predict values for sphere radii cannot be attributed to experimental error alone.

Table 1. Analysis of Variance Table for a 2nd Order Model With Sphere Diameter as the Dependent Variable.

Source	D.F.	Sum of Squares	M.S.	F Ratio
Sum of squares for b_1, b_2	2	98,940	49,470	738
Sum of squares for b_{11}, b_{22}, b_{12}	3	83,590	27,863	418
Residual	6	15,350		
Lack of fit	3	15,150	5,050	76
Error	3	200	67	
Total	11	197,880		

Model – $\hat{y} = b_0 x_0 + b_1 x_1 + b_2 x_2 + b_{11} x_1^2 + b_{22} x_2^2 + b_{12} x_1 x_2$.*

*Independent variables x_1, x_2 are ammonia and water concentrations, respectively.

Complications arose primarily while investigating the lower concentrations of water and ammonia. The shaded portion of Figure 4 indicates this as the region of fusing ellipsoids. In this lower concentration region the silica flocculated in irregular ellipsoidal particles and began to fuse into rod-like filaments. For reasons beyond the scope of this investigation it proved to be impossible to produce spheres with average diameters less than 90 nm with the ethanol-TEOS system. A brief attempt was made to produce smaller uniform spheres with the methanol-TMOS system. The initial screening tests were unsuccessful and produced rod-like filaments comprised of 20 to 50 nm ellipsoidal particles.

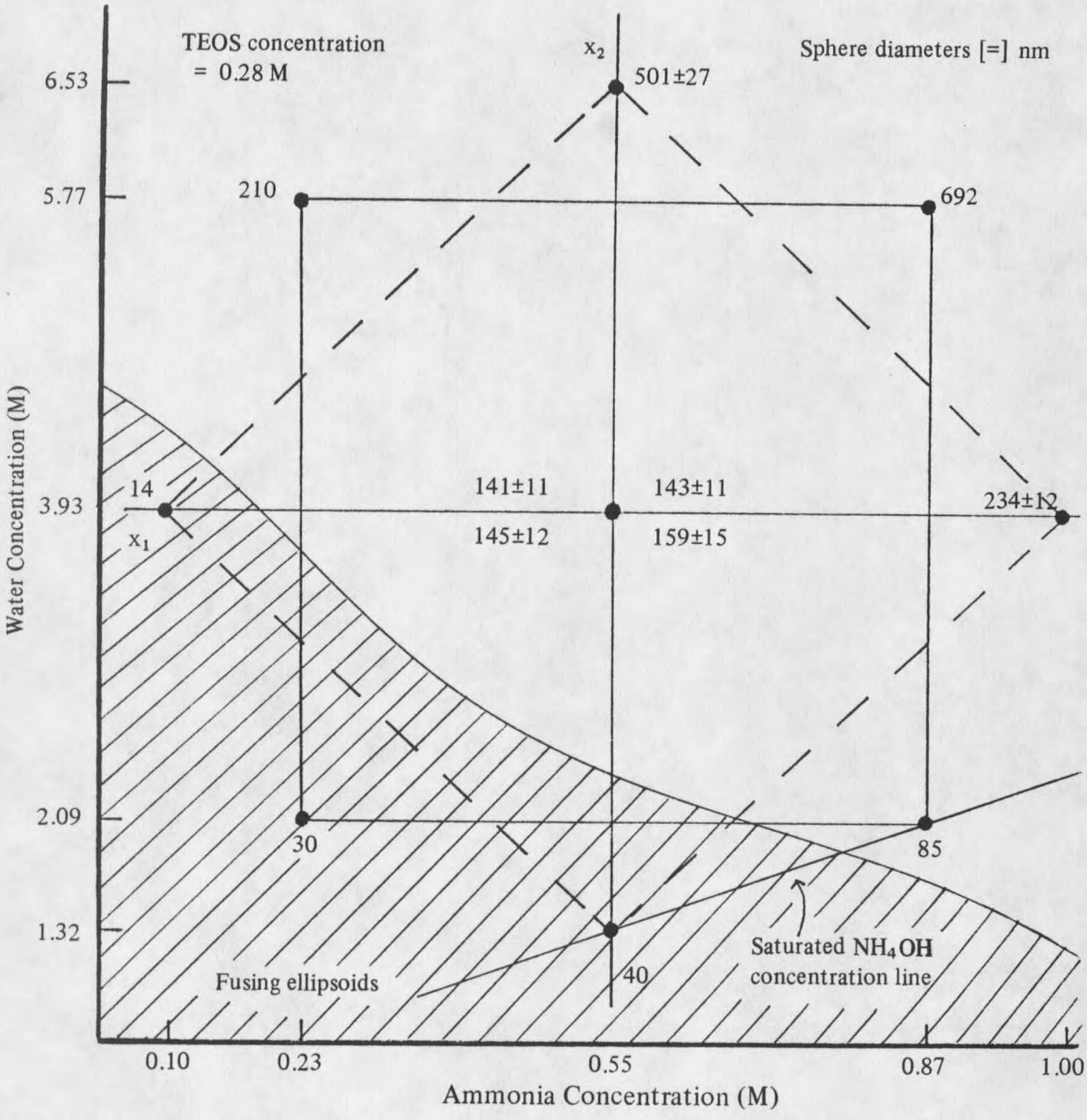

Figure 4. Response surface octagon for TEOS-ethanol system.

The octagonal center points of Figure 4 do indicate, however, the high degree of reproducibility of the sphere growth scheme. The concentrations of reactants and resulting sphere sizes are presented in Table 2. The average sphere diameters of batches 1, 2, and 4 are seen to be in very close agreement with an average of 143 ± 7 nm. The diameter reported for batch No. 3 is somewhat in doubt due to the small sample population size. (This resulted from complications in developing TEM micrographs for batch No. 3.)

Table 2. Comparison of Response Surface Octagon Center Point Sphere Sizes.

	Reaction Mass Concentration For All Batches				
Reagent	NH_4OH	H_2O	TEOS	ETOH	Total Volume
Molar (ml) conc	0.55 (3.7)	3.9 (4.7)	0.28 (6.2)	(85.4)	100.0
Batch No.	1	2	3	4	Average
Sphere diam. (nm)	141 ± 11	145 ± 12	159 ± 15	143 ± 11	147 ± 6
Spheres measured	195	237	44	202	678

Having encountered difficulty developing the second order surface response model, it was decided to try a set of straightforward experiments with the ethanol-TEOS system in which the ammonia concentration would be independently varied with the only water added to the system being that added with the saturated ammonium hydroxide solution itself. By maintaining a TEOS concentration of 0.28 M, these experiments simply represent an extension of the saturated ammonium hydroxide line depicted in Figure 4 to a concentration of 2.0 M ammonia. The particles produced at ammonia concentrations from 1.4 to 2.0 M were monodisperse at a given concentration and spherical, with average diameters ranging from 249-611 nm. The results are presented in Table 3. It is readily apparent that within the concentration limits of this set of experiments the average sphere diameter is directly related to the amount of ammonia and water present.

The size range resulting from these experiments was broad enough to produce a significant change in the average pore radius calculated using Equation 11. Spheres formed

Table 3. Response of Sphere Size to Varying Ammonia and Water Concentrations in the TEOS-Ethanol System.

NH_4OH (M)	H_2O (M)	Ave. Sphere Diameter (nm)
1.0	2.4	100*
1.4	3.4	249 ± 16
1.6	3.8	320 ± 23
1.8	4.3	453 ± 29
2.0	4.8	611 ± 55

*Estimated diameter based on sample size less than 20 particles.

under the conditions from 1.4 to 2.0 M ammonia were later to be used in fabricating model porous pellets.

The 100 nm spheres produced at 1.0 M ammonia exhibited surfaces substantially more uneven than those at higher concentrations. It is thought that the lower ammonia and/or water concentration limit was again being approached, producing problems similar to those encountered with the response surface model at the low concentrations. In an attempt to produce a set of monodisperse 100 nm diameter spheres a random set of tests was conducted—again by varying the ammonia and water concentrations in the ethanol-TEOS system. The results of these experiments indicated that a suitably monodisperse set of spheres, with an average diameter of 100 nm, could be produced at concentrations of 0.55 M ammonia and 3.0 M water. The results of four batches of these concentrations are listed in Table 4. Figure 1 is a micrograph of batch No. 2. The close agreement of these results again indicates the excellent reproducibility of the sphere-growth scheme. Spheres produced at these concentrations were also later used to fabricate the porous pellets.

In summation, it was shown to be significantly easier to produce monodisperse sets of spheres in the 100 nm to 1000 nm diameter size range than to form spheres with diameters less than 100 nm. Stöber et al. produced spheres with average diamters in the 50 nm to 80 nm size range using the pentyl-ester and an ethanol solvent. To increase the flexibility of a model porous media and to insure a Knudsen diffusion mechanism at relatively

Table 4. Comparison of Average Sphere Diameters at Reaction Conditions Producing Approximately 100 nm Diameter Spheres.

	Reaction Mass Concentrations For All Batches				
Reagent	NH_4OH	H_2O	TEOS	ETOH	Total Volume
Molar (ml) conc	0.55 (3.7)	3.0 (3.0)	0.28 (6.24)	(87.1)	100.0
Batch No.	1	2	3	4	Average
Sphere diam. (nm)	103 ± 9	94 ± 8	98 ± 8	107 ± 10	100 ± 4
Spheres measured	371	499	302	444	1616

high pressures with higher molecular weight gases, it would be necessary to develop porous media using spheres with less than 100 nm diameters. Continued investigations with other combinations of tetra-esters and a variety of alcoholic solvents would be in order. However, with low molecular weight gases and at relatively low pressures the 100 nm to 600 nm diameter spheres generated with the ethanol-TEOS system described above will serve nicely as building blocks for the model porous media.

Fabricating and Characterizing the Model Porous Pellet

Experimental Apparatus and Procedure

Preparing the Slurry of Spheres. The spheres must be dried before being pressed into assemblages of fixed geometry. A gelatinous material was often observed resting on the bottom of the 250 ml Erlenmeyer flasks. Upon inspection with the electron microscope this appeared to be a matrix of spheres embedded in an amorphous silica gel-like substance. This contamination was effectively removed by carefully decanting the slurry of spheres from the flasks, leaving the undesired material behind.

The slurry of spheres was next placed under 25 inches of vacuum at 303 K and evaporated to dryness using a Büchi Rotovapor R110 rotary vacuum system. The dried spheres were removed from the evaporation flask and placed in an agitation apparatus used to break up flakes or lumps which tended to form during the drying period.

Figure 5 pictures this device which consisted of a rubber stoppered-1000 ml-vacuum flask, a magnetic stirring device and a nitrogen gas purge system. A magnetic stir bar was made to rock in the bottom of the flask for approximately 24 hours. A slow purge of nitrogen gas insured against water vapor diffusing into the flask from the atmosphere. A piece of glass tubing was tightly fitted into the one-holed stopper. A Gelman micropore filter (0.1 μm pore size) was attached to the end of the glass tubing which protruded into the flask. This served to catch spheres which became entrained by the nitrogen purge gas. The rubber stopper was clamped securely onto the lip of the flask as the system pressure was maintained at 10 psig. At the end of this stage a small sample of the dried powder was resuspended for examination using the T.E.M. techniques described earlier. Micrographs taken of the original reaction mass slurry were then compared with those taken of these resuspended spheres. The remaining dried spheres were now removed from the vacuum flask and placed in tightly sealed glass storage flasks.

Determining the Density of the Spheres. The true density of the silica spheres was determined allowing the calculation of pellet porosity by use of Equation 14. The density was determined by directly measuring the volume of a known weight of spheres. First, the density of a liquid (methanol or water) was experimentally determined at 273 K by measuring the weight of a known volume of this liquid contained in a 25 ml volumetric flask. A quantity of spheres was next placed in the tared flask and the weight of the spheres was recorded. The flask was filled to the proper volume with the above liquid. The temperature was allowed to equilibrate at 273 K.

The final weight of the flask was now determined. The difference between the weight of the flask full of liquid, with and without spheres, yields the weight of liquid displaced and consequently the volume displaced by the spheres. This volume is the true volume of the spheres, and the density could now be calculated.

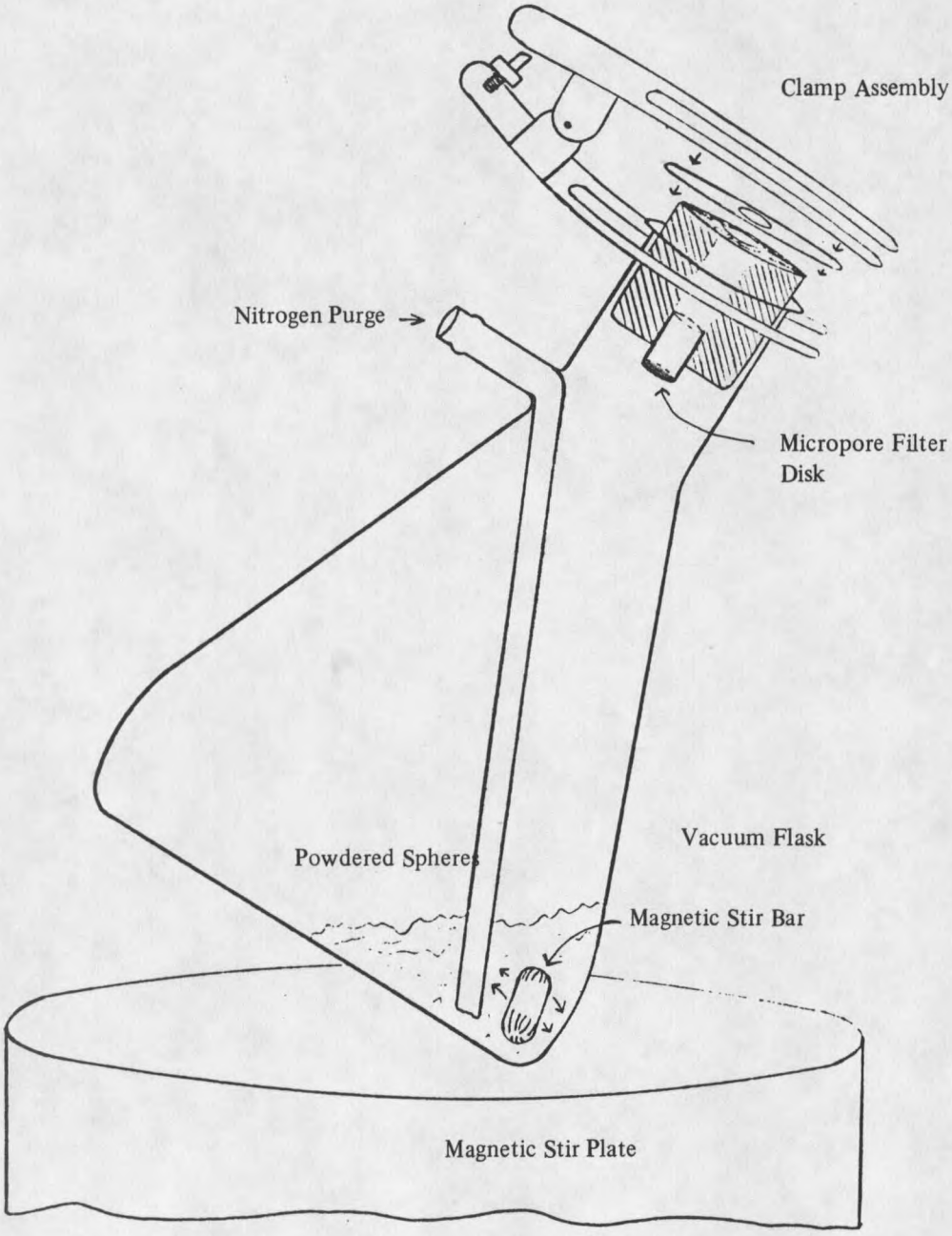

Figure 5. Agitation apparatus employed to reduce flakes and lumps formed during the drying process.

Pelleting Procedure. To actually form the pellet of model porous media, the dried spheres were packed into stainless steel cylinders. Each cylinder was cut from 0.635 cm-316 S.S. tubing with a standard wall thickness of 0.089 cm. The cylinders were cut on a lathe to ensure square ends, after which each was engraved with an identification symbol. The length was approximately 1.2 cm and was accurately determined, along with the inside diameter, by measuring with a micrometer. The tare weights were also recorded at this time.

The pellets were pressed using a modified Rimac Spring Tester hand press depicted in Figure 6. The press was fitted with a plunger (4340 alloyed steel) which fit into the cylinders with 0.008 cm clearance. The cylinders were held in place by resting in a stainless steel seat, notched to fit onto the pad of the press. The applied pressure could be varied continuously from 1,000 to 10,000 psia by observing the pressure indicated on the dial on the front of the press. The dried spheres were introduced into the top of the cylinder and the desired pressure was applied for approximately 10 seconds. To insure isotropic pellet formation small amounts of spheres were added to the cylinder between successive pressings. Depending on the sphere diameters between 20 and 35 pressings were used per cylinder. The cylinders were slightly over filled by fitting a piece of rigid plastic tubing onto the top of the cylinder, thus allowing compaction above the upper rim. The plastic sleeve was subsequently removed and the excess material was shaved off the top (and bottom if necessary) with a single edged razor blade. This procedure ensured that the proper total volume was being achieved. The cylinders were carefully wiped free of loose spheres and fingerprint oils and then weighed to determine the weight of spheres packed into the known volume. The porosity of each pellet was now calculated using Equation 14 with the known weight of spheres, the volume of the cylinder and the true density of the silica material.

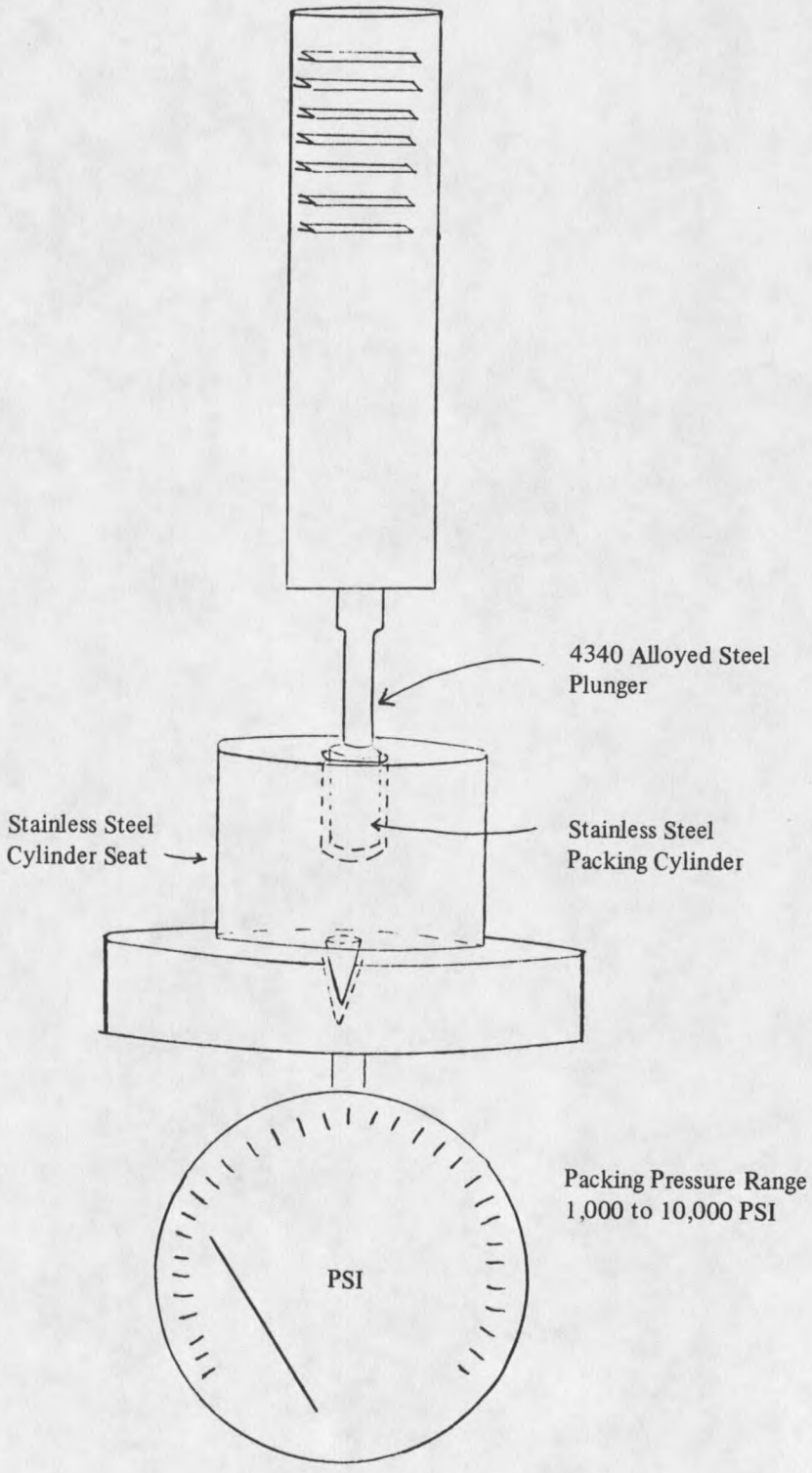

Figure 6. Schematic of pellet pressing apparatus.

Results and Discussion

Spheres in Powder Form

The micrographs of resuspended spheres are indistinguishable from those taken when the spheres were newly formed. Figures 7 and 8 are respective micrographs of spheres taken before and after the drying process. These figures indicate that the spheres are undamaged due to attrition in the rotovac system. They also show that the lumps and flakes have been completely broken down by the agitating magnetic stir bar. Therefore, the drying steps successfully produce a powder of uniform spheres which are in a form suitable for pellet formation. However, because the process requires the materials to be transferred between vessels a number of times, the overall yield of product is relatively low. It is theoretically possible to produce about 2.5 grams of silica per 100 ml batch using a TEOS concentration of 0.28 M. Typically, actual yields measured between 0.4 and 0.6 grams per batch, resulting in an average yield around 20%. Although this yield may seem low for a controlled laboratory process, no significant attempt was made to modify the process due to the combination of relatively low cost reagents and also the ease and speed with which a new batch could be generated.

True Density of the Spheres

The true density of the silica was measured twice with methanol as the solvent and once with water. The average of the three measurements was $1.89 \pm .02$ g/cm^3. This is the value which was used in Equation 14 to calculate the porosity of all the pellets. The results of the three investigations are recorded in Table 5.

The calculated solvent densities were within 0.3 percent of the accepted book values at 273 K, thus indicating the accuracy of the technique employed. The use of two different solvents was an attempt to indicate if the spheres were being completely wetted. There was no significant difference between the densities and it was, therefore, assumed that both

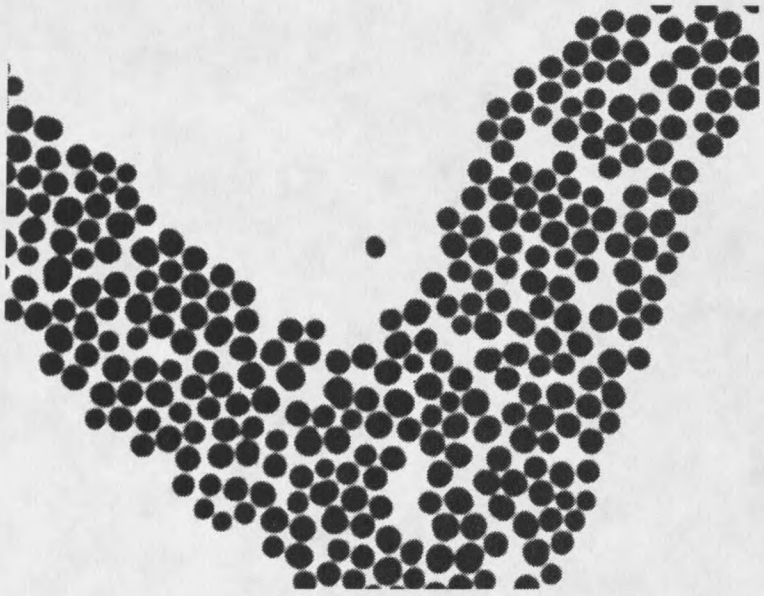

Figure 7. Typical TEM micrograph taken preceding the drying process (107 nm diameter spheres, 33,000x).

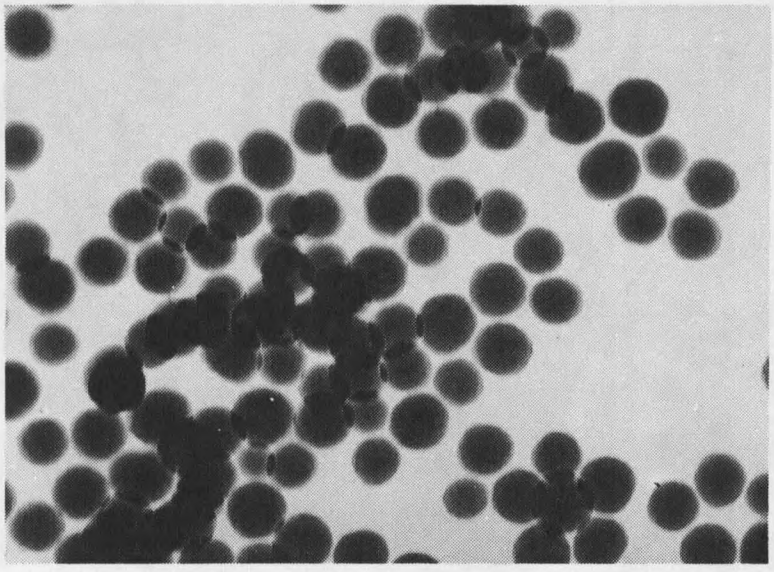

Figure 8. Typical TEM micrograph taken following the drying process (107 nm diameter spheres, 65,000x).

Table 5. Comparison of Silica Sphere Density Measurements.

Solvent (273 K)	Calculated Density of Solvent (g/cm^3)	Weight of Spheres (g)	Calculated Density of Spheres (g/cm^3)
MEOH	0.811 ± .0009	2.4326 ± .0002	1.83 ± .03
MEOH	0.808 ± .0009	5.1795 ± .0005	1.92 ± .03
H_2O	0.998 ± .0011	4.0962 ± .0004	1.93 ± .03

liquids wet the surface completely. There is no apparent reason as to why the two methanol densities should vary slightly, although the difference in sample size may have had an effect.

Commonly, the density values reported for amorphous silica range from 2.1 to 2.2 g/cm^3 [54]. Due to the nature of this particular reaction Iler [26] has suggested, however, that while the particles are growing, voids may develop within the spherical structure. One could speculate that this was the case with these particular spheres, and that these void regions are contributing to the approximate 10% decrease from the literature value. It is interesting, however, that the voids or irregularities were not visible on the surface of the spheres even when viewed carefully under high magnification (i.e., see Figure 3).

Pressing the Pellet

The stainless steel cylinders averaged 0.2 cm^3 in volume and generally weighed about 1.4 grams. No volume changes were noticed due to repeated packing at high pressure.

Pellets were generated using packing pressures from 1,000 to 10,000 psi. At pressures less than 1,000 psi the structural integrity of the pellet was doubtful, particularly if it was necessary to remove the pellet from the cylinder for subsequent use in the diffusion measuring apparatus. Therefore, most of the pellets were produced at 10,000 psi, which was the maximum obtainable pressure using this diameter plunger in our press. Figure 9 is a scanning electron microscope (SEM) photograph of the interior surface of a pellet

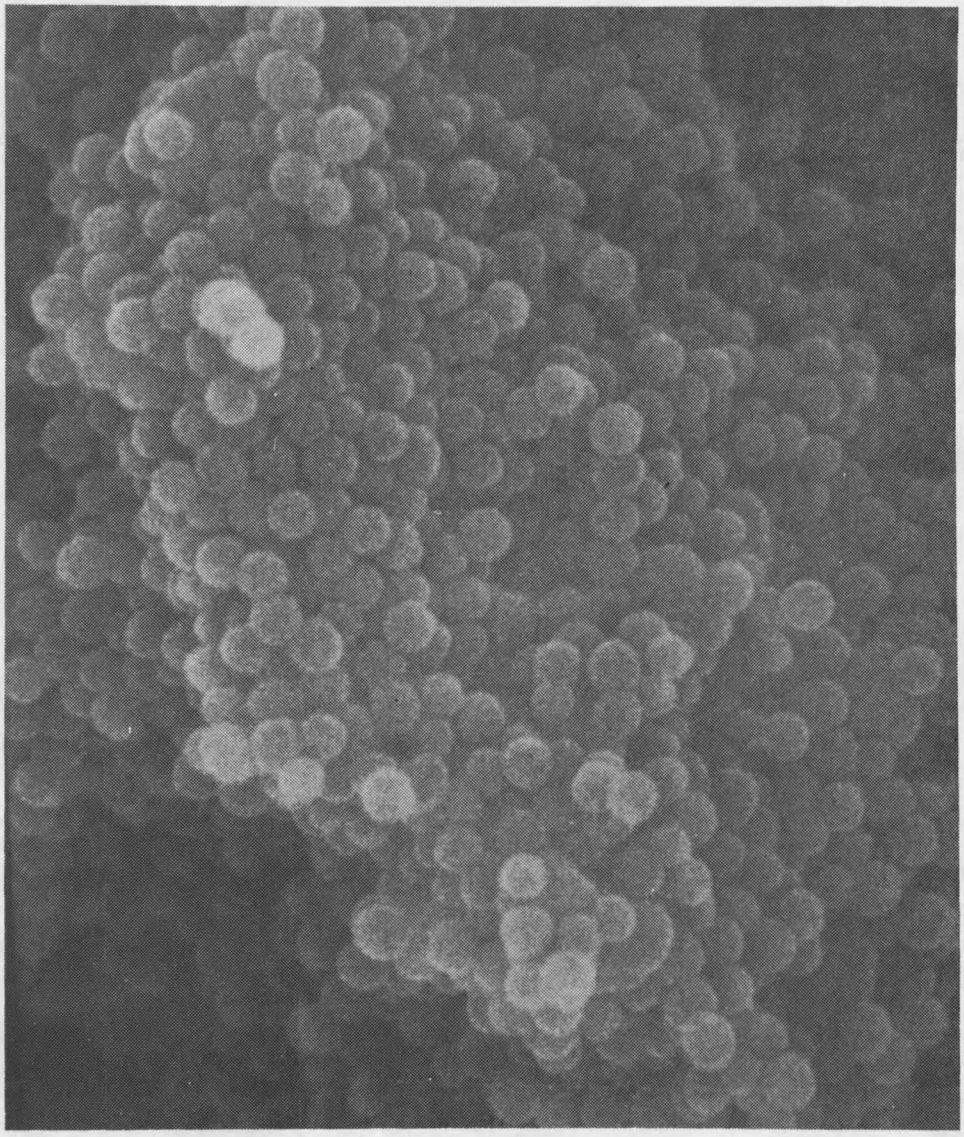

Figure 9. SEM photograph of the interior of a pellet pressed at 10,000 psi (ϵ = 0.35, 40,000x).

pressed at 10,000 psi. The individual spheres are seen to remain intact at this upper limit of packing pressure. Various pellets were randomly sectioned and SEM photography revealed isotropic structure throughout the length of the pellets.

For pellets packed at 10,000 psi the average porosity was 0.363 ± .030. This value is in close agreement with the literature values of 0.359-0.375 reported by Haughey and Beveridge [37] for a close random packing of spheres. Table 6 indicates the expected independence of porosity with respect to sphere size. The slightly low value of 0.331 ± .025 reported for the 103 nm spheres was thought to have been caused by moisture contamination from the ambient air. Also, it must be pointed out that each average sphere diameter reported had its own unique size distribution. The average porosity must certainly be a function of this size distribution. Populations skewed toward the smaller size spheres would exhibit lower than predicted porosity because of the ability of the relatively small spheres to fill voids inaccessible to larger spheres.

Table 6. The Response of Average Porosity to Changing Sphere Size.

Sphere Diameter (nm)	No. of Pellets Formed	Average Porosity*
103 ± 9	8	.331 ± .025
107 ± 10	5	.377 ± .028
249 ± 16	6	.381 ± .027
320 ± 23	7	.366 ± .026
453 ± 29	9	.364 ± .024
611 ± 55	7	.359 ± .024

*Pelleting pressure = 10,000 psi.

The porosity was found to be a very weak function of pressure in the pressure range from 1,000 to 10,000 psi. Figure 10 indicates an approximate 15% decrease in pellet porosity with a 1000% increase in packing pressure. For all practical purposes one could say that in this pressure range the porosity is only a very weak function of packing pressure.

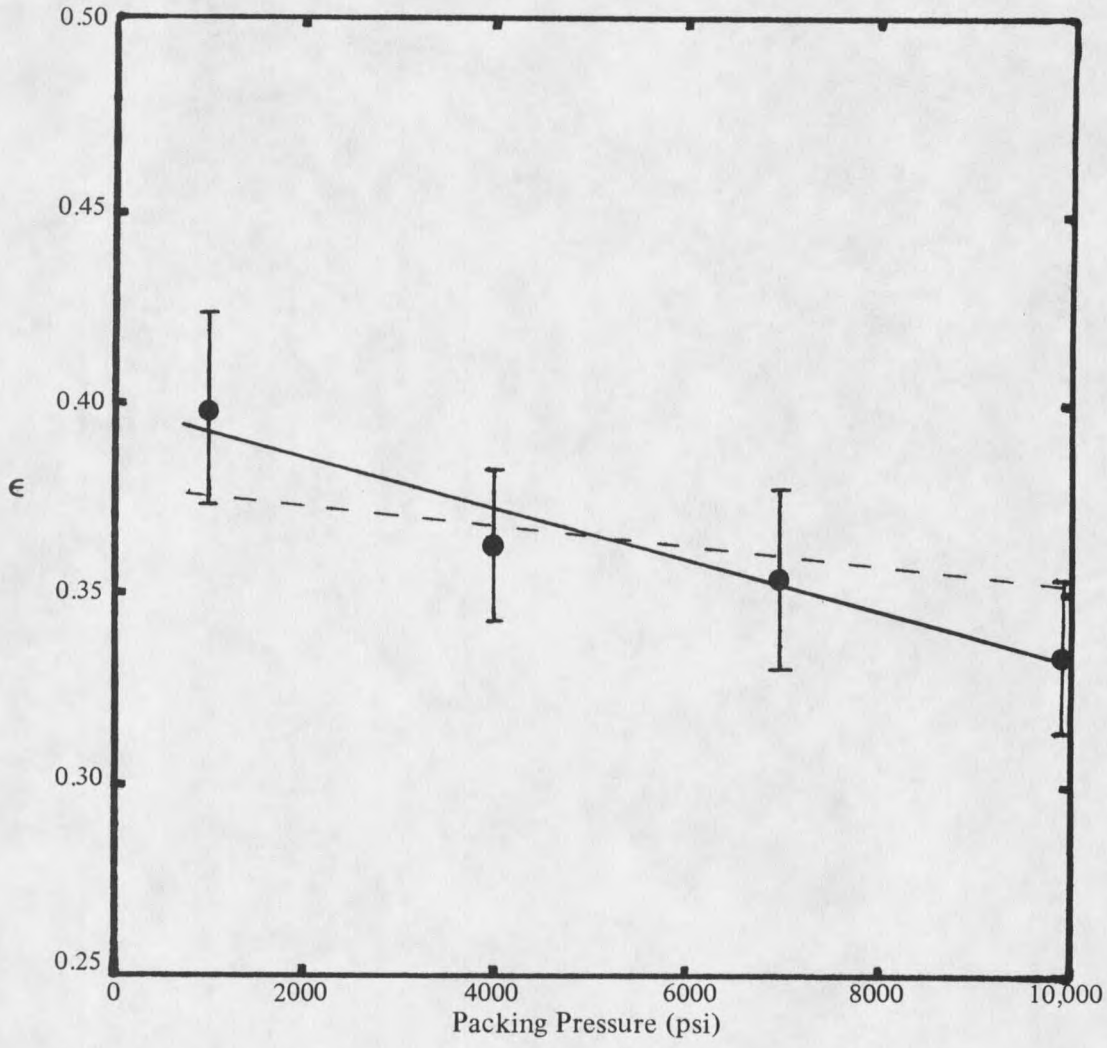

Figure 10. Response of pellet porosity to increased pelleting pressure.

DETERMINATION OF EFFECTIVE DIFFUSIVITIES IN BEDS OF RANDOMLY PACKED UNIFORM SPHERES

Apparatus

A "plug flow" apparatus was constructed for the purpose of measuring the Knudsen diffusivities of low molecular weight gases through a model porous media. Major requisites of the design were the flexibility to operate over a range of total inlet pressures less than 1 atmosphere, the ability to control and maintain a constant sample temperature, and the ability to continuously measure the extremely slow flux through the sample. After various early modifications the final apparatus, constructed of 0.317 cm stainless steel tubing and brass or stainless valves, can be represented schematically by Figure 11.

It was necessary to maintain differing constant internal-inlet pressures from 80 to 400 torr. This was effected by use of a Matheson Model 70 regulator (R_2). Inlet pressure to this internal pressure regulator was maintained at 5 psig by the gas cylinder regulator (R_1). The ambient air reference pressure port of the Matheson regulator was attached to a vacuum source of less than 80 microns. The outlet pressure (internal-inlet pressure) was, therefore, effectively reduced from psig to psia. The desired operating internal-inlet pressure could then be varied by adjusting the tension on the regulator diaphram. Use of Equation 15 necessitates a knowledge of pressures both upstream (internal-inlet) and downstream (outlet) of the sample pellet. A simple mercury manometer was employed to measure the ΔP across the sample. A Varian Model 801 thermocouple vacuum gauge (G_2) was used to monitor the system pressure downstream of the pellet. Given this reference pressure and the manometer ΔP, the actual internal-inlet pressure could be determined by difference. In addition, a rough indication of the internal operating pressure was also

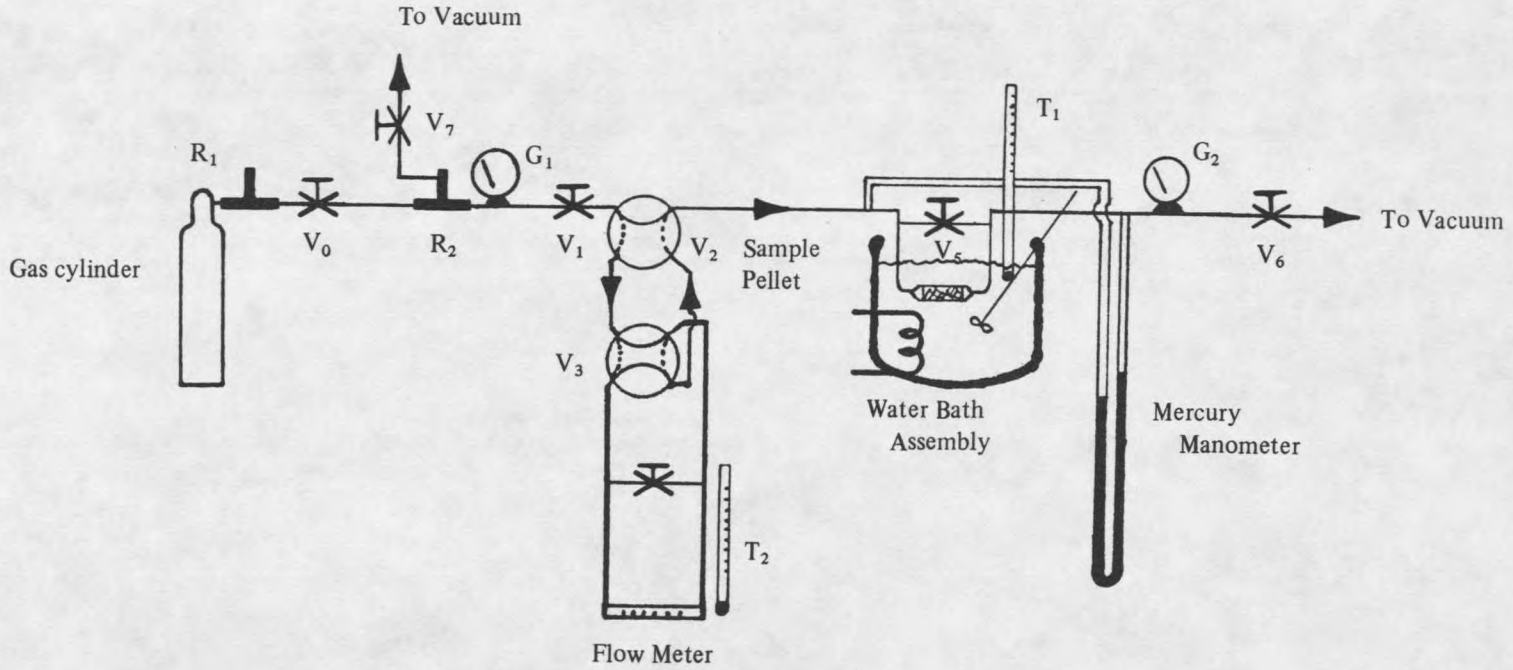

Figure 11. "Plug flow" diffusion apparatus.

available from an Ashcroft vacuum gauge (G_1) attached immediately following the internal pressure regulator.

The sample temperature was maintained at 303 K by immersion in a VWR Model 1120 circulating-constant temperature-water bath. The sides and top of the bath were insulated and the temperature (T_1) varied less than ± 0.1 K throughout the investigations.

The flux could be measured by timing a di-butyl phthalate bubble as it traveled in a 1.0 cm^3 glass pipet. This pipet was connected horizontally in line to the 0.316 cm stainless tubing by Cajon Ultra-Torr fittings. By use of a Whitey 4-way ball valve (V_3), the direction of flow in the pipet could be switched from one direction to the other. This provided continuous flux monitoring capability under equilibrium operating conditions. A second Whitey ball valve (V_2) was incorporated to allow complete by-pass of the flow meter assembly during start up and shut down phases.

Experimental Procedure

The sample porous pellet was affixed in position in the water bath between two pieces of 0.317 cm stainless tubing connected to the inlet and outlet, respectively. A jig was constructed which held these two sample connecting tubes in a position similar to that of operating conditions in the bath. This facilitated easy installation of new sample pellets by avoiding repeated drainage of the water bath.

First, it was necessary to remove the pellet from the stainless steel cylinder in which it was packed. This was accomplished by shrinking a length of 0.635 cm electrical shrink-loc tubing onto the cylinder with 1 cm of tubing extending beyond each end of the cylinder. This tubing was then further shrunk onto the two sample connecting tubes. The entire surface of the shrink tubing and an adjacent 0.5 cm of the stainless tubing was then sealed with silicone caulking compound. This assembly was next attached to the system via

swage lock fittings. The pellet was then degassed by maintaining a ΔP across the pellet-jacket assembly of approximately 400 torr using helium as a carrier gas. The combined vacuum and gaseous flux tended to slightly free the pellet from the steel jacket. The internal surface of the cylinder is relatively rough compared with the sphere sizes and it is speculated that a small number of spheres were dislodged by bulk gas flow at the interface between the pellet and the cylinder. The evacuated condition would help to remove water molecules which may have adsorbed onto the surfaces and caused a swelling of the pellet. At the end of an approximately 12 hour period the assembly was disassembled and the pellet could generally be removed with a very slight pressure applied to one end of the pellet. The final length and cross sectional area of the pellet were now recorded.

The pellet was next inserted into a length of 0.312 cm shrink-loc tubing, 1 cm longer than the pellet on each end. This tubing was shrunk onto the two sample holding tubes while positioned in the jig. Again, the assembly was sealed with silicone caulking and reattached in the water bath. The system was now ready for start up.

Four gases (hydrogen, helium, nitrogen and argon) were studied as they diffused through a number of different pellets. As a general procedure, a gas was chosen and hooked up to the system with the given pellet secured in line. The following steps detail the procedure of measuring the flux through a pellet:

1. V_0 was closed and all other valves were opened. The system was then evacuated overnight while the pellet equilibrated in the constant temperature bath.
2. V_2 was positioned to by-pass the flow meter assembly.
3. V_7 was closed and the diaphram spring was adjusted to produce the desired operating pressure.
4. V_6 was closed and V_7 was opened. This was to avoid atmospheric pressure air from contaminating the system. At an outlet pressure less than 100 microns V_6 was opened.

5. V_0 and V_1 were opened. The inlet gas was now allowed to flow freely as V_5, the pellet by pass valve, remained open. The regulator would now come to a dynamic equilibrium position. G_1 indicated if the correct tension was applied to the diaphram spring.
6. V_5 was closed. The system was now in an operational mode although the flow meter assembly was still by-passed. The pressure must now be equilibrated between the system and the flow meter assembly.
7. V_1 and V_6 were closed. V_2 was slowly positioned to include the flow meter assembly. If the valve was opened too rapidly, a ΔP would develop across the flow meter bubble, due to the inability of the V_4 by-pass line to accommodate the rapid increase in pressure. The bubble would then be forced rapidly in one direction and be dispersed on the walls of the pipet. If the liquid would not coalesce and reform a bubble the flow meter would have to be disassembled and a new bubble would be introduced.
8. Steps 5-7 were repeated until pressure equilibrium was reached. This was usually accomplished in 3 to 4 sequences. At this point the system was allowed to reach final equilibrium. This generally took about 1 hour, during which time the vacuum was properly established on the downstream side of the pellet and the internal-inlet pressure regulator would adjust to its final operating position.
9. V_4 is closed and the volumetric flow rates are monitored. Usually 4 flow rates (two in each direction) were recorded. The temperatures T_1 and T_2 were recorded, along with the ΔP and the readings of gauges G_1 and G_2. Equation 15 was now used to calculate an effective diffusivity. The outlet concentration, C_2, was taken to be zero throughout all calculations.
10. To change pressures, steps 2-9 were repeated.

11. To shut down the system, the flow meter assembly was by-passed, V_1 and V_6 were closed, V_5 opened and the pellet holder assembly could be removed.

Results and Discussion

A series of preliminary investigations were conducted to establish standard operating conditions under which the Knudsen diffusion mechanism would predominate. The primary considerations were to operate at the lowest available internal-inlet pressure and the highest reasonable sample temperature-conditions generating the longest possible mean free paths for the four experimental gases. A standard operating temperature of 303 K was chosen as being a sufficiently high temperature to contribute positively to the λ values while also being close enough to ambient temperature to reduce large water losses due to evaporation throughout an experimental run. It was also thought that this temperature was high enough to ensure a minimal amount of surface adsorption by any of the gases, thus retarding a surface diffusion contribution.

It was determined that the internal-inlet pressure regulator limited the lower end operating pressure to approximately 80 torr. Because the Knudsen diffusivity is a function of the mean free path and the average pore radius it was necessary to make a comparison of these values in the pressure range somewhat above 80 torr. Table 7 displays the experimental gases and their respective average mean free paths at 100 and 400 torr and 303 K. An average pore radius generated using Equation 11 and a pellet constructed of the largest spheres (radius 305 nm) is approximately 118 nm. This value is approaching the λ values at 400 torr and would indicate the necessity of remaining below this operating pressure.

If the Knudsen diffusion regime is operational in the pressure range from 80 to 400 torr, the experimentally determined effective diffusivity should be constant and independent of operating pressure. Figure 12 indicates that over this pressure range this is essentially the case for our system of gases and a pellet constructed of 305 nm radius spheres.

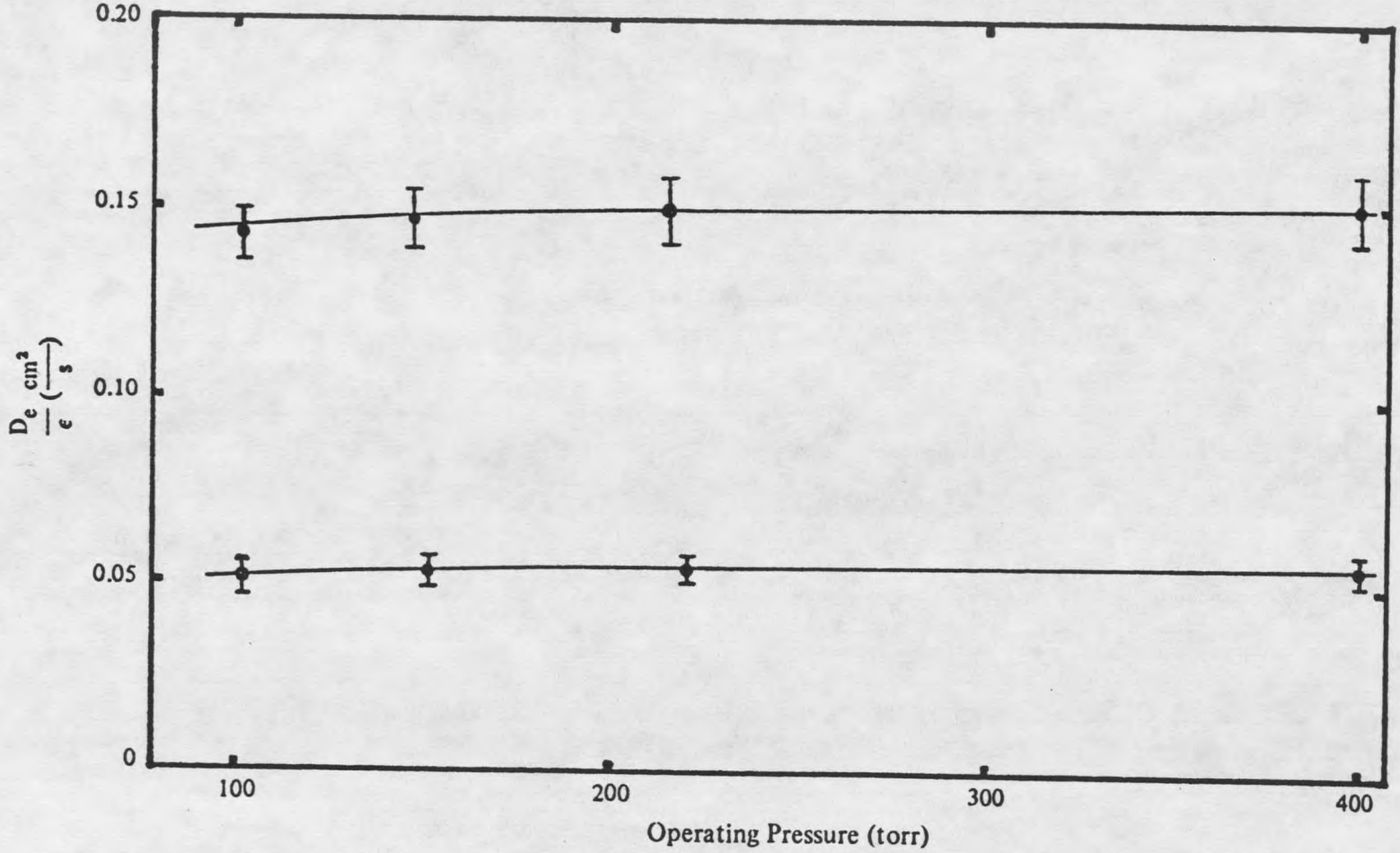

Figure 12. The response of effective diffusivity to increased operating pressure.

Table 7. Experimental Gases with Corresponding Mean Free Paths at 303 K.

Gas	MW	λ_{nm}, 100 torr	λ_{nm}, 400 torr
Argon	39.9	560	140
Nitrogen	28.0	490	123
Helium	4.0	1090	273
Hydrogen	2.0	880	220

The two gases plotted, helium and nitrogen, have the longest and shortest mean free paths, respectively. The effective diffusivity was seen to increase slightly for both gases with increased pressure, averaging 8% for a 300% increase in operating pressure. This is anomalous to the prediction that as the transition region between Knudsen and bulk diffusion is approached, the effective diffusivity decreases. This apparent contradiction was due, however, to the relative pressure drop through the system. The flux over the pressure range remained essentially constant and, therefore, produced a relatively constant pressure drop through the system's valves and swage-lock connections. At the lower pressures this was a relatively larger percentage of the total operating pressure. A correction factor could be established to account for the pressure drop, however, the correction insignificantly effects the results of the investigation and redesign of the system was deemed to be unnecessary. Having established that the effective diffusivities in this pressure range are independent of operating pressure would indicate that any pressure in this range would serve as a standard operating condition. In an attempt to ensure reasonable operation of the internal-inlet pressure regulator and to maximize the mean free paths of the gases, 100 torr was chosen as the operating pressure throughout the investigations.

As a means to further substantiate a transport mechanism dominated by Knudsen diffusion, and as a way to correlate a large amount of data, a plot of D_e/ϵ versus $\sqrt{T/MW}$ was formed. Equation 4 indicates that for a given pellet such a plot will yield a straight line if the diffusion mechanism is Knudsen. The effective diffusivity should be independent of which type of gas molecule(s) (i.e., monatomic or diatomic) are in use and should be a

function of molecular weight only, given a constant temperature system. Although the four gases chosen are all relatively low in molecular weight, the differences are enough to give the abscissa of the plot a substantial spread. The results of measuring effective diffusivities in seven different porous pellets are displayed in Figure 13. The sphere radii ranged from 52 to 305 nm. All seven pellets were seen to exhibit the straight line behavior predicted by Equation 4 and a Knudsen-dominated diffusion mechanism. As was expected and predicted by kinetic theory, the measured diffusivities increased with increased average pore radius, generated by forming pellets from spheres of increased radius. Table 8 points out the reproducibility of the data, as duplicates of two sphere sizes were subsequently run. Each duplicate pellet was identical in measurable physical parameters since the porosities were essentially the same. The resulting effective diffusivities varied less than 2% for each of the sphere sizes.

Table 8. Reproducibility of Effective Diffusivities in Similar Pellets.

Pellet Number	Sphere Radius (nm)	ϵ ±6%	D_e/ϵ ± 7%		
			Nitrogen	Helium	Hydrogen
6	160 ± 11	0.367	–	0.326	0.451
7	160 ± 11	0.366	0.118	0.332	0.448
8	226 ± 14	0.360	0.182	0.503	0.704
9	226 ± 14	0.364	0.184	0.498	0.705

The interesting thing to note as a result of this reproducibility between different pellets of the same sphere size is that for a constant porosity a constant tortuosity factor also results. This points to a "similarity" of internal structure even though it has been formed in a completely random fashion. This finding is significant because it is a necessary prerequisite to basing a general tortuosity factor on the hydraulic average pore radius parameters of sphere size and porosity.

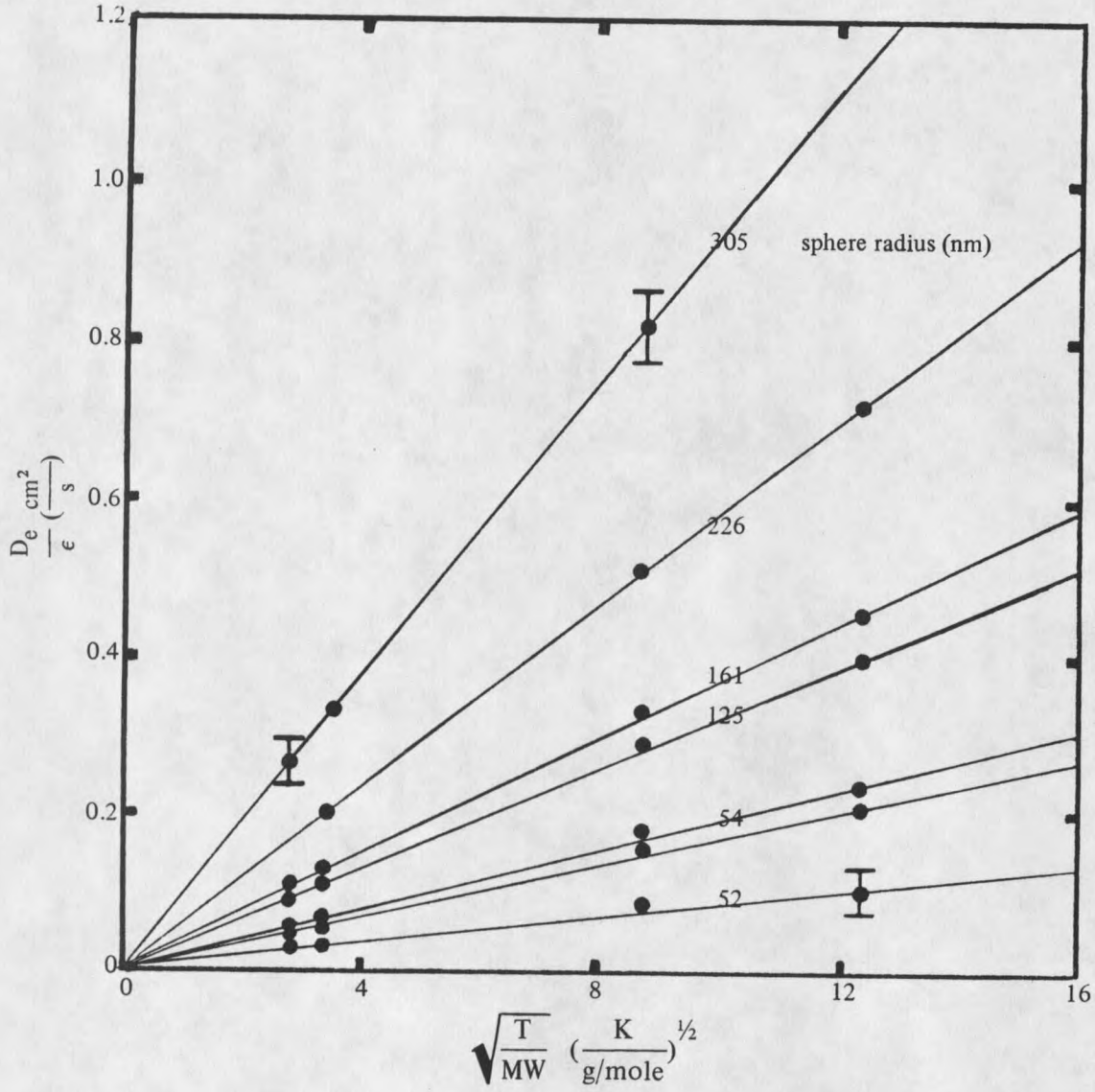

Figure 13. Effective diffusivities determined using a series of increasing molecular weight gases diffusing through pellets of increasing average sphere size.

The tortuosity factor was estimated using a plot of D_e/ϵ versus average pore radius, $\bar{r}$, where $\bar{r}$ was calculated using Equation 11 and the porosities and sphere radii for the series of pellets tested. The data used to generate these plots is summarized in Table 9.

Table 9. Raw Data for Tortuosity Calculations.

Pellet Number	Ave. Sphere Radius (nm)	ϵ ±6%	$\bar{r}$ (nm) Eq. 11	Argon	Nitrogen	Helium	Hydrogen
				$D_e/\epsilon \pm 7\%$ (cm^2/s)			
4	52	0.324	17	0.024	0.030	0.080	0.107
3	54	0.340	18	0.046	0.056	0.151	0.202
1	54	0.377	22	0.051	0.061	0.172	0.228
5	125	0.386	52	0.085	0.101	0.280	0.390
6	160	0.367	62	0.100	–	0.326	0.451
8	226	0.360	86	0.155	0.182	0.503	0.704
2	305	0.364	116	0.213	0.261	0.707	–

Plots of this data for argon and hydrogen are displayed in Figures 14 and 15, respectively. Both figures reveal that D_e/ϵ is a linear function of $\bar{r}$, which is predicted by Equation 6. This being the case, Equation 4 can be substituted into Equation 6 and this combination can be rearranged in the following manner to allow calculation of the tortuosity factor.

$$\frac{D_e}{\epsilon} = \frac{.00097}{\tau}\sqrt{\frac{T}{MW}}\,\bar{r} \tag{16}$$

Estimation of the tortuosity factor for a given gas is now reduced to the simple matter of calculating the slopes of the lines represented in Figures 14 and 15. The slopes for all four gases were determined from the data in Table 8 using a least squares regression including the origin. Slopes and average tortuosities are listed in Table 10. The average tortuosity factor of 1.47 ± .10 is essentially constant for all four gases within the error limits of the calculations.

It is interesting to compare this result with the tortuosity factor of 1.40 found by Smith and Huizenga [12] (see Appendix A) when using this same hydraulic radius in conjunction with monte carlo simulations with beds of uniform spheres packed to 0.37 porosity

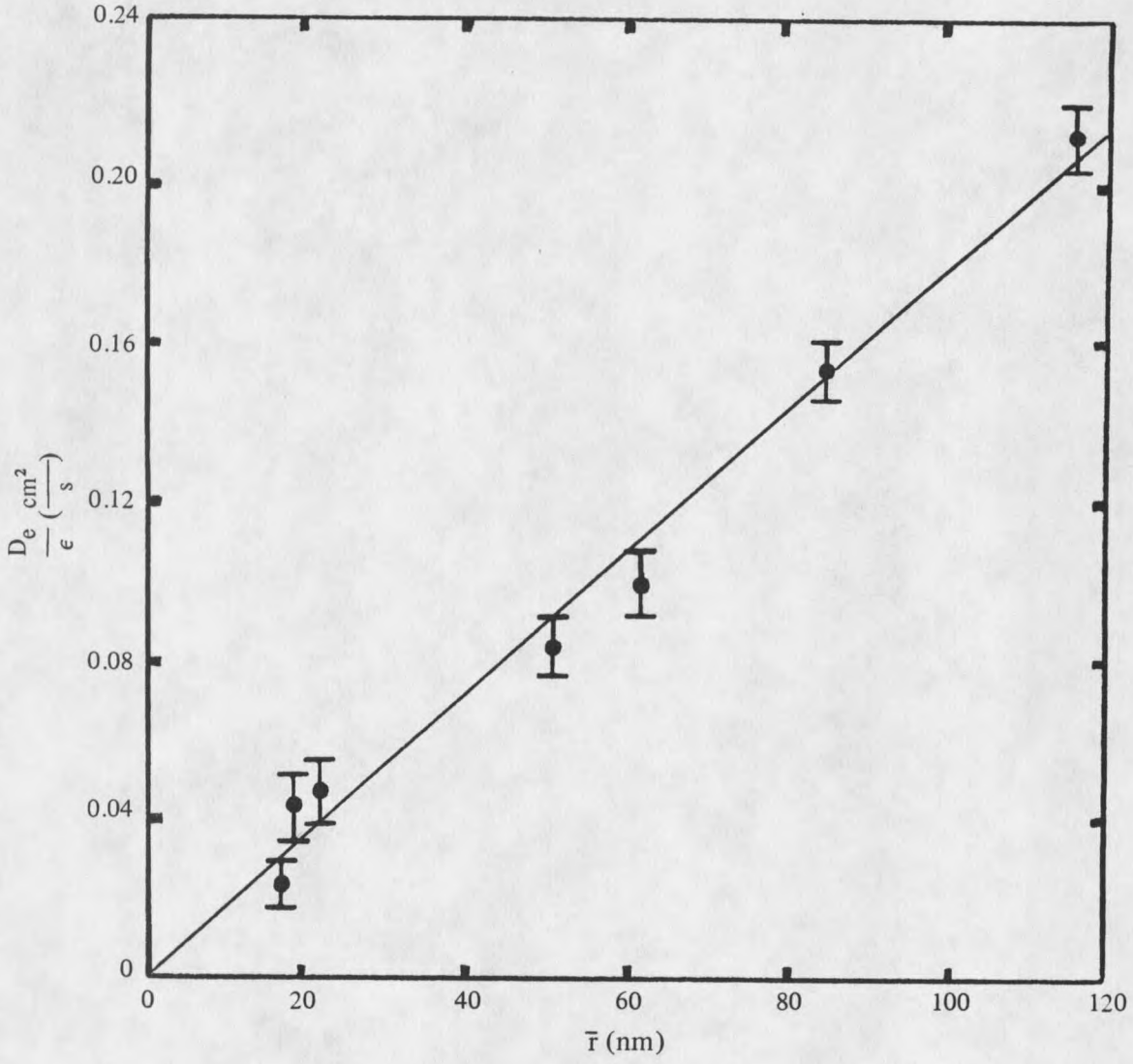

Figure 14. Argon effective diffusivity as a function of increased average pore radius ($\bar{r}$ = hydraulic radius via Equation 11).

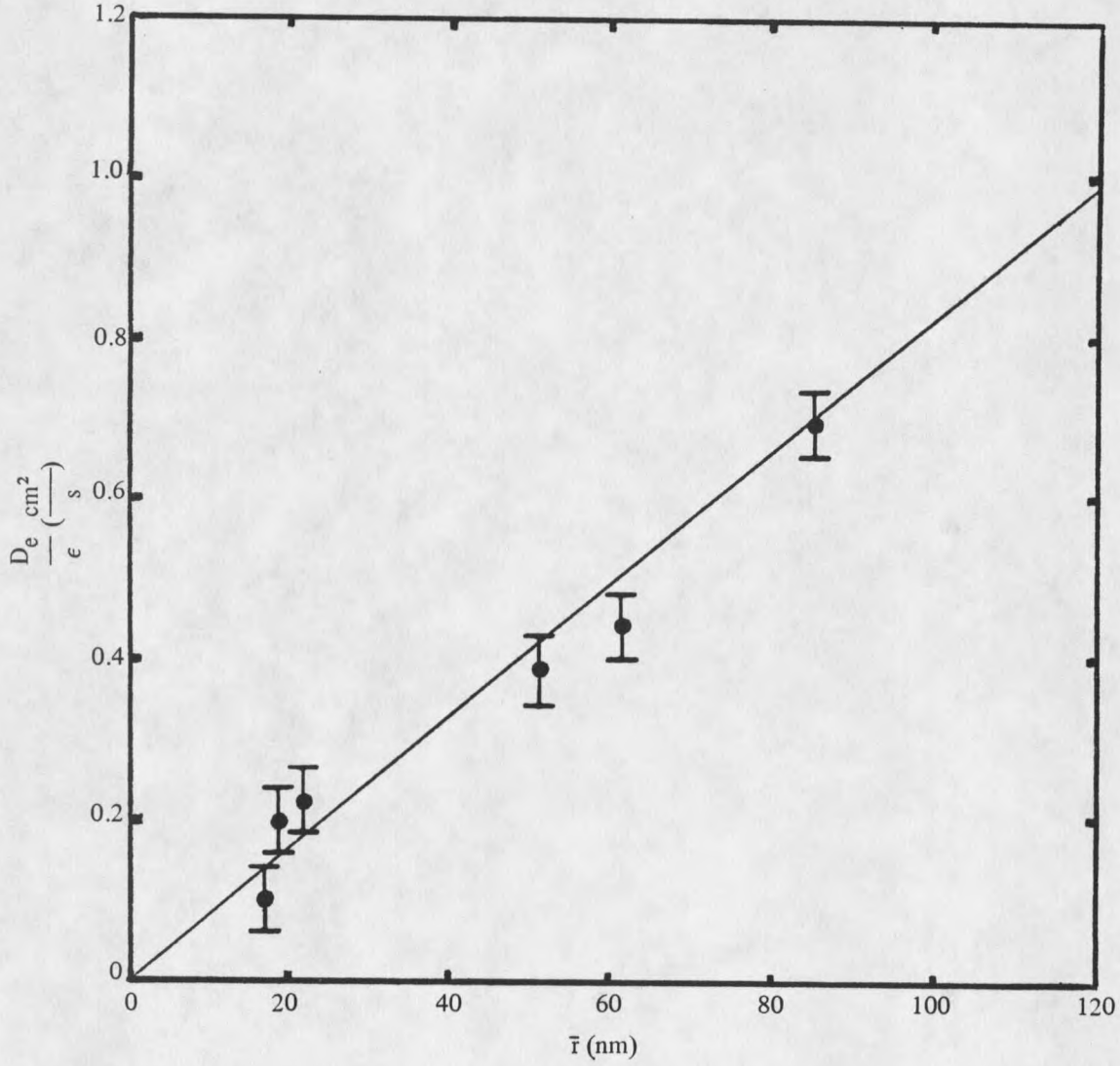

Figure 15. Hydrogen effective diffusivity as a function of increased average pore radius ($\bar{r}$ = hydraulic radius via Equation 11).

Table 10. Average Tortuosity Factors for the Four Experimental Gases.

Gas	Slope ($\frac{cm}{s}\sqrt{g/K} \times 10^{-7}$)	Tortuosity ± 7%
Argon	0.00176	1.51
Nitrogen	0.00215	1.48
Helium	0.00579	1.46
Hydrogen	0.00821	1.45

These values are both essentially identical to Wheeler's initial theoretical value of $\sqrt{2}$ based on pores being, on average, 45 degrees from the direction of flow. This implies that when the hydraulic radius is employed, no effect due to the non-ideal shape of the pore is realized. It is not readily apparent why these values are in such close agreement. It is, however, thought provoking, and these results provide a basis for further investigation, both experimental and theoretical.

As was noted in the introduction, if the average pore radius were based on mercury porisimetry or sorption isotherm data the radius determined could be a factor of 1.5 smaller than that hypothesized by the hydraulic radius model. If, in addition, the tortuosity factor $1/\epsilon$ (used in the absence of other information regarding τ) were employed, the predicted transport rates would be approximately 4 times smaller than those actually measured experimentally.

SUMMARY

1. It was possible to produce a monodisperse set of silica spheres in the sub-micron size range using an ammonium hydroxide catalyzed ethanol-TEOS (tetraethyl orthosilicate) system. Sets of spheres were produced with individual batch average sphere diameters ranging from 100 nm to 600 nm.
2. For a given batch of spheres the standard deviation in particle diameter was, on average, 7 to 9 percent.
3. The sphere growth scheme was seen to be very reproducible as spheres of a desired size could be repeatedly generated given the same reaction conditions.
4. By pressing, dried spheres could be formed into pellets with known dimensions. The average porosity of the pellets, $0.36 \pm .03$, coincided with literature predicted values and was found to be independent of sphere size. The porosity was also found to be essentially independent of packing pressure when the applied pressure was in the range of 1,000 to 10,000 psi.
5. A "plug flow" apparatus was constructed with which to measure the effective Knudsen diffusivity of a series of increasing molecular weight gases (hydrogen, helium, nitrogen, argon) as they diffused through a single porous pellet. Standard operating conditions for the system were a temperature of 303 K and a ΔP of 100 torr across the sample pellet.
6. A series of pellets constructed from sets of monodisperse spheres with radii ranging from 52 to 305 mm were studied. For each pellet, a plot of D_e/ϵ versus $\sqrt{T/MW}$ was formed for a series of gases. In substantiation that diffusion was in the Knudsen regime, these plots were linear for each pellet.

7. Duplicate pellets were investigated, and the effective diffusivities were found to vary by less than 2 percent. This finding, pointing to a basic similarity of internal structure in randomly packed beds of spheres, allows for the calculation of a general tortuosity factor to be used with pellets constructed from sets of uniform spheres over a range of sphere sizes.
8. For each gas a tortuosity factor was estimated from a plot of D_e/ϵ versus the average pore radius, where the average pore radius was defined as the hydraulic pore radius and was a function of the easily determined parameters of sphere radius and pellet porosity. The plots were linear, as predicted by kinetic theory, and the average tortuosity, 1.47 ± .10, was independent of the type of gas employed.
9. The average tortuosity of 1.47 ± .10 compares identically (within the error limits of the experimentation) to Wheeler's theoretical value of $\sqrt{2}$ and to the value of 1.40 obtained through simulation by Smith and Huizenga [12].
10. If the average pore radius were calculated via mercury porisimetry or sorption isotherm techniques (methods which would yield average pore radii approximately ½ that of the hydraulic radius), and if, in the absence of information concerning the value of a tortuosity factor a value of $1/\epsilon$ was used, an effective transport rate as much as 400% in error would be predicted.

RECOMMENDATIONS FOR FUTURE RESEARCH

1. The use of the highest grade reagents and extremely clean reaction vessels would probably aid in narrowing the size distribution of an individual batch of spheres. This would become increasingly important if this work was extended to a study in of tortuosity factors in beds of bidisperse spheres.
2. Mixing various quantities of different sized spheres might produce pellets of varying porosity. It would be of interest to study Knudsen diffusivity in beds of porosities both higher and lower than 0.36.
3. It would be advantageous and of considerable interest to use a model porous media as constructed in this investigation to study both surface and liquid diffusion rates.
4. There is a need to compare the hydraulic radius tortuosity factor with those generated using both mercury porisimetry and sorption isotherm techniques. Perhaps further research with various methods of generating average pore radii would shed insight into the most accurate manner in which to model less ideal porous media.

REFERENCES CITED

REFERENCES CITED

1. Satterfield, C. N., *Mass Transfer in Heterogeneous Catalysis*, M.I.T. Press (1970).
2. Weisz, P. B., Chem. Tech., 504 (1973).
3. Satterfield, C. N. and Cadle, P. J., I and EC Process Design and Development, Vol. 7, No. 2 (1968).
4. Smith, J. M., *Chemical Engineering Kinetics*, McGraw-Hill, N.Y. (1970).
5. Knudsen, M., Annal. Physics, *285*, 73 (1928).
6. Wheeler, A., in Emmett P. H. (ed.), *Catalysis, Vol. 2*, Rheinhold, N.Y. (1955).
7. Abbasi, M. H., Evans, J. W. and Abramson, I. S., AIChEJ, *29*, 4, 617 (1983).
8. Johnson, M. F. L. and Stewart, W. E., J. Catalysis, *4*, 248 (1965).
9. Wiggs, P. K. C., in *The Structure and Properties of Porous Materials*, Everett, D. H. and Stone F. S. (eds.), Academic, New York, 1958, p. 193.
10. Wakao, N. and Smith, J. M., Chem. Eng. Sci., *17*, 525 (1962), Ind. Eng. Chem. Fund. Quart., *3*, 123 (1964).
11. Ruckenstein, E., Vaidyanathan, A. S. and Youngquist, G. R., Chem. Eng. Sci., *26*, 1305 (1971).
12. Smith, D. M. and Huizenga, D. G., Proceedings of the 10th IASTED International Symposium on Modelling and Simulation, In Press (1984).
13. Ritter, H. L. and Drake, L. C., Ind. Eng. Chem., Anal. E., *17*, 787 (1945).
14. Lowell, S., *Introduction to Powder Surface Area*, J. Wiley & Sons, New York (1979).
15. Brunauer, S., Mikhail, R. S. and Boder, E. E., J. Colloid. Int. Sci., *24*, 451 (1967).
16. Brunauer, S., Emmett, P. H. and Teller, E., J. Am. Chem. Soc., *60*, 309 (1938).
17. Haughey, D. P. and Beveridge, G. S. G., Can. J. ChE., *47*, 130 (1969).
18. McCabe, W. L. and Smith, J. C., *Unit Operations of Chemical Engineering*, 3rd Ed., McGraw-Hill, Inc., New York (1976).
19. Stöber, W. and Fink, A., J. Colloid Interface Sci., *26*, 62 (1968).

20. Mason, G., J. Colloid Sci., *35*, 279 (1971).

21. Fitch, R. M. (ed.), *Polymer Colloids*, Plenum Press, N.Y. (1971).

22. Watillon, A. and Dauchot, J., J. Colloid Interface Sci., *27*, 507 (1968).

23. Demchak, R. and Matijević, E., J. Colloid Interface Sci., *31*, 257 (1969).

24. Brace, R. and Matijević, E., J. Inorg. Nucl. Chem., *35*, 3691 (1973).

25. Matijević, E., Budnik, M. and Meites, L., J. Colloid Interface Sci., *61*, 302 (1977).

26. Iler, R. K., *The Colloid Chemistry of Silica and Silicates*, Cornell Univ. Press, Ithaca, N.Y. (1955).

27. Iler, R. K., Surface Colloid Sci., *6*, 1 (1973).

28. Cohan, H. D. and Setterstrom, C. A., Ind. Eng. Chem., *39*, 1364 (1947).

29. Aelion, R., Loebel, A. and Firich, F., J. Am. Chem. Soc., *72*, 5705 (1950).

30. Cadle, J. P. and Satterfield, C. N., Ind. Eng. Chem. Fund., *7*, 192 (1968).

31. Satterfield, C. N. and Saraf, S. K., Ind. Eng. Chem. Fund., *4*, 451 (1965).

32. Hoogschagen, J., Ind. Eng. Chem., *47*, 906 (1955).

33. Scott, G. D., Nature, *194*, 956 (1962).

34. Bernal, J. D., Nature, *183*, 141 (1959).

35. Bernal, J. D., Nature, *185*, 68 (1960).

36. Blum, E. H. and Wilhelm, R. H., Proceedings of the AIChE-IChemE joint meeting, Symposium No. 4, pp. 4-21, London, June 13-17 (1965).

37. Haughey, D. P. and Beveridge, G. S. G., Chem. Eng. Sci., *21*, 905 (1966).

38. Bernal, J. D., Proc. Roy. Soc., *A280*, 299 (1964).

39. Lamb, D. E. and Wilhelm, R. H., Ind. Eng. Chem. (Fund.), *2*, 193 (1963).

40. Steinour, H. H., Ind. Eng. Chem., *36*, 618, 840, 901 (1944).

41. Scott, G. D., Nature, *188*, 908 (1960).

42. Carman, P. C., T. I. Chem. E., *15*, 150 (1937).

43. McGreary, R. K., J. Am. Ceramic Soc., *44*, 513 (1961).

44. Bernal, J. D., Mason, J. and Knight, K. R., Nature, *194*, 959 (1962).

45. Denton, W. H., A.E.R.E. Report E/R 1095 (1957).

46. Smith, W. O., Physics, *1*, 18 (1931).

47. Haynes, H. W. Jr. and Sarma, P. N., A.I.Ch.E.J., *19*, 1043 (1973).

48. Drake, M. C., Master's Thesis, Dept. Chemical Engineering, Montana State Univ. July (1984).

49. Schneider, P. and Smith, J. M., A.I.Ch.E.J., *14*, 762 (1958).

50. Dogu, G. and Smith, J. M., Chem. Eng. Sci., *31*, 123 (1970).

51. Wicke, E. and Kallenbach, R., Kolloid. Z., *97*, 135 (1941).

52. Smith, D. M., Ph.D. Thesis, Dept. Chem. Eng., Univ. New Mexico, May (1982).

53. Hunter, J. S., Chem. Eng. Progr. Symposium Ser. 31, *56* (1960).

54. Weast, R. C. (ed.), *Handbook of Chemistry and Physics*, 56th Ed., CRC Press, Cleveland (1975).

APPENDICES

APPENDIX A

SIMULATION OF KNUDSEN DIFFUSION IN POROUS MEDIA

SIMULATION OF KNUDSEN DIFFUSION IN POROUS MEDIA

Douglas M. Smith
David G. Huizenga

Department of Chemical Engineering
Montana State University
Bozeman, MT 59717 USA

ABSTRACT

When gases diffuse through porous media at low pressures or when the characteristic pore size is of the same order as the mean free path, transport is dominated by molecule-pore wall collisions. This phenomena, known as Knudsen diffusion, is of interest in a number of engineering applications such as catalysis and combustion. Kinetic theory provides insight concerning Knudsen diffusion in capillaries. However, for porous media which is not described by a single pore size, the proper choice for the Knudsen diffusivity is not clearcut.

This work employs Monte Carlo simulation techniques to study Knudsen diffusion in porous media. The porous media is assumed to be comprized of a random packing of spheres of a single diameter. The porous media is created by randomly inserting spheres into a matrix and checking to ensure that the new sphere does not intersect any other sphere. Porous solids with porosities between .39 and .54 are created in this manner. Monte Carlo methods are used to determine the rate of transport, and hence the Knudsen diffusivity, through the solid. The relationship between the effective Knudsen diffusivity and the pore size, which would be measured experimentally, is obtained. From this information, tortuosity factors are calculated.

INTRODUCTION

The transport of gases through porous media is of interest for a wide range of engineering applications. These include catalysis, combustion, sorption, gas separations and nuclear waste isolation. In porous solids which exhibit relativly small characteristic pore sizes, the actual reaction rate(combustion rate, etc.) may be fixed by mass transfer limitations. Therefore, considerable interest exists for predicting the extent of these limitations given a knowledge of the pore network and the nature of the diffusing gas.

When gases are migrating through porous media, several different mechanisms may exist. These include bulk, Knudsen, surface and configurational diffusion[1]. Transport in the bulk diffusion regime is governed by molecule-molecule collisions. Knudsen diffusion occurs at lower pressures and in smaller pores where transport is dominated by molecule-pore wall interactions(ie. gas mean free path >> pore size). When the diffusing gas adsorbs, surface transport of adsorbed molecules may facilitate the overall migration rate. When the pore and molecules are of the same order, the transport rate is governed by specific pore wall-molecule interactions(configurational diffusion).

Of particular concern to this investigation is the phenomenon known as Knudsen diffusion or molecular streaming. When the characteristic pore size is much smaller than the mean free path of the diffusing gas, migrating gas molecules are more likely to intersect the pore wall rather than other gas molecules. Since the distance that a molecule will travel before striking a pore wall is a function of both the pore radius and the molecule's velocity, one would expect that the magnitude of D_k is related to the pore radius. For diffusion in capillaries at low pressure, Knudsen[2] has derived the following expression for D_k:

$$D_k = \frac{4r}{3}\sqrt{\frac{2RT}{\pi M}}\ \frac{(2-f)}{f} \qquad (1)$$

where: D_k = Knudsen diffusivity.
f = Fraction of molecules which stick to the pore wall.
M = Molecular weight.
r = Pore radius.
R = Gas constant.
T = Temperature.

For practical applications, the sticking coefficient, f, is usually taken to be 1 and Eq. 1 is simplified in cgs units[3] to:

$$D_k = 9700\ r\sqrt{\frac{T}{M}} \qquad (2)$$

Knudsen's findings cannot be applied for the calculation of diffusivities in porous solids unless some type of pore model is assumed. The simplest model commonly used for the study of gas transport in solids is the parallel pore model proposed by Wheeler [4]. In this model, all pores are assumed to be cylindrical and of the same diameter. The effective diffusivity is therefore given by:

$$D_e = \epsilon D_k / \tau \qquad (3)$$

where: ϵ = Porosity.
τ = Tortuosity factor.

The diffusivity, D_k, may be calculated using Equation 2 for transport in the Knudsen regime. The tortuosity factor accounts for the fact that pores are not always parallel to the flow direction and of cylindrical shape. For solids of practical interest, the value of τ is usually between 1 and 8[5].

The pore structure of many solids cannot be

represented as bundles of uniform cylinders. In particular, the pore structure of many solids more often resemble the void volume contained in an assemblage of spheres. This assemblage of spheres pore model may be taken to represent the opposite limiting case of pore structure(as compared to cylindrical pores). Many catalyst supports and sorbents are actually manufactured via the agglomeration of silica and/or alumina sols. When examined under an electron microscope, these materials appear to be a random packing of spheres with diameters of the same order. Figure 1 is a scanning electron micrograph (SEM x40,000) of a pellet cross-section manufactured from 97 nm silica microspheres.

Figure 1. Random assemblage of spheres (x40,000).

BACKGROUND

Numerous studies of the effect of pore shape deviations from the idealized cylinder have been undertaken and are reviewed by Satterfield[5]. However, these investigations are strictly valid for transport in the bulk diffusion regime only. Studies of Knudsen diffusion in random media have been conducted by assuming that the pore structure is a series of interconnecting cylinders of different diameters[6]. This type of analysis ignores entrance/exit effects at the junctions between pores of different diameters which could result in significant errors in the calculated effect of pore shape nonuniformity. Additionally, the complexity and large number of parameters for this type of model makes it's application difficult.

Knudsen diffusion in beds of overlapping spheres has been considered by Strieder and Aris[7] using a variational approach. An upper bound on the Knudsen permeability, which is related to D_k, was obtained. Their calculations appear to agree with experimental measurements reported by Carman[8] only at high porosities. This is probably related to the use of the overlapping spheres model.

The use of Monte Carlo simulation techniques to simulate Knudsen diffusion in porous solids appears to have been pioneered by Evans, Abbasi and co-workers[9,10]. In those works, porous solids are assumed to be comprized of a mixture of solid sphere sizes placed into a regular matrix. By using several sizes of a spheres, porosity values lower than the limiting value of .36-.40(for uniform spheres placed randomly) may be obtained. From simulations performed over a wide range of porosities, the characteristic length for Knudsen diffusion was found to be:

$$k_o/\bar{d} = .0093 + .1\epsilon - .0181\sigma/\bar{d} \qquad (4)$$

where the Knudsen diffusivity is defined as:

$$D_k = \frac{4}{3}\sqrt{\frac{8RT}{\pi M}}\, k_o \qquad (5)$$

and: $\bar{d}$ = Mean pore size.
k_o = Characteristic length.
σ = Pore diameter standard deviation.

The major problem with the application of Equations 4 and 5 is the question of the proper choice for the mean pore radius. Pore size analysis is usually conducted using mercury porosimetry, analysis of adsorption isotherms or a combination of the surface area and total pore volume. For this last method, the mean pore diameter is defined as:

$$\bar{d} = \frac{4V}{SA} \qquad (6)$$

In principle, pore diameter values calculated via Equation 6 and mercury porosimetry/sorption analysis will be in agreement for cylindrical pores only. However, for beds of uniform spheres, pore diameters can vary by a factor of 2 between the two methods. Pore sizes determined via mercury porosimetry/sorption analysis represent the smallest cross-section of a nonuniform pore[11]. In contrast, Equation 6 represents what might be considered a "true" average pore size. Evans and co-workers used a stereological technique for theoretically measuring the pore size distribution of their simulated porous solids. However, it is unclear how these values are related to values that one would obtain from actual measurements. With beds of uniformly sized spheres, certain of these questions may be addressed since Equation 6 may be reduced to a function of the sphere diameter and porosity only:

$$\bar{d} = \frac{2\epsilon}{3(1-\epsilon)}\, d_s \qquad (7)$$

The average pore diameter that one would obtain using porosimetry for a random packing of spheres with $\epsilon = .37$ has been calculated by Mason[12] to be $.275\, d_s$.

CALCULATION SCHEME-MODEL SOLID

When uniformly sized spheres are poured into a container, the porosity or void fraction of the resulting fixed bed is invariably between .36 and .40[13]. A number of schemes such as polyhedral models, coupled sphere models, local sphere shell models and Monte Carlo methods have been proposed for simulating this process[14].

For this work, a Monte Carlo simulation was used to randomly place spheres into a container(in a mathematical sense). A set of x, y and z coordinates corresponding to a sphere center are randomly chosen. The container is than searched to ensure that the sphere center location is acceptable(ie. no overlapping spheres). This process is then repeated until the desired porosity is obtained or an excessive number of trials is required.

A major problem with the use of Monte Carlo methods for this type of simulation is the

large number of insertion trials which become necessary as the limiting porosity value is approached. This problem was minimized by using a relatively small model solid and a search technique. For our work, a cubic container with sides equal to 10 d_s was used. This appeared to be the minimum size necessary to avoid edge effects in our diffusion simulations. The distance between each new desired set of sphere center coordinates and all previously placed centers must be calculated to ensure that no overlapping occurs. In our scheme, we decrease the required number of distance calculations by a factor of 37. This is accomplished by dividing the container into 1000 cubes with dimensions of 1 d_s. Each set of sphere center coordinates has an additional set of three integers which define the subblock that it is located in. When checking a new set of coordinates, distance calculations must be undertaken only for the neighboring 27 subblocks that surround the center. Although this revised search method does not reduce the number of insertion trials necessary to place a particular sphere into the matrix, it does increase the speed of calculating a trial.

As discussed above, the number of insertion trials, N, necessary to find a satisfactory location for a new sphere center increases with decreasing porosity. This is illustrated in Figure 2, a plot of the average # of insertion trials versus porosity for a 10x10x10 matrix.

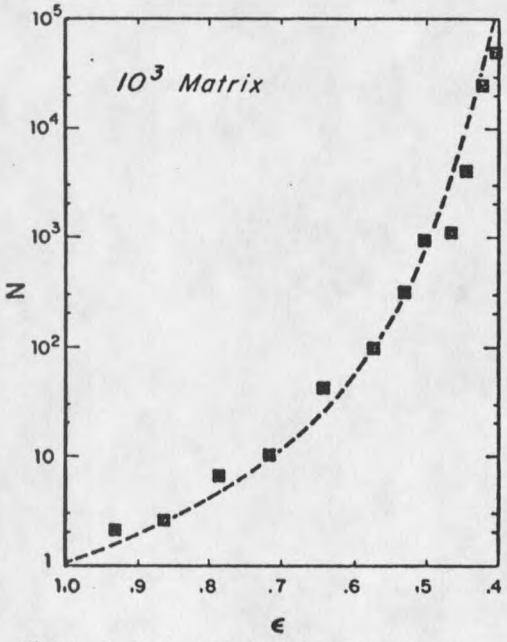

Figure 2. Number of insertion trials as a function of matrix porosity.

For this investigation, 5 porous solids have been simulated using a DEC VAX 11/750 computer equipped with a floating point processor. Execution time ranged up to 16 hours for a 10x10x10 solid with a porosity of .384. Random sets of sphere center coordinates are selected using the uniform random number generator[0,1] of the multiplicative congruential type associated with DEC's extended Fortran feature[15]. For solids fabricated from spheres of a single diameter, the calculation of the porosity is directly related to the number of sphere centers which fit into the container. Our 5 simulated solids exhibited porosities ranging from .386 to .543.

CALCULATION SCHEME-DIFFUSION SIMULATION

Our simulation of Knudsen transport presumes that a concentration(pressure) gradient is imposed across our porous solid in one direction. The pressure on one side of the solid is taken to be P, and a vacuum is maintained on the opposite side. A molecule which enters the solid may either be transmitted through the solid to the vacuum side or reflected back to the high pressure side. In either instance, a large number of molecule-wall collisions may occur before the molecule ultimately leaves the solid. The effective diffusivity, D_e, may be related to the fraction of molecules, f_t, which will penetrate a certain distance, L, into the solid via a flux balance[9]:

$$D_e = \frac{f_t}{4}\sqrt{\frac{8RT}{\pi M}}\,L \qquad (8)$$

In order to find the effective diffusivity and hence, D_k and τ, Equation 8 is used. Plotting f_t versus the reciprocal penetration length(1/L), a straight line with slope proportional to D_e is obtained.

The random movement of molecules through the model solid is carried out on a step by step basis. To start the simulation, a set of coordinates on the high pressure side of the solid are randomly selected. The simulation is started at a distance of 1 d_s away from the solid. Three direction cosines(α, β, γ) are selected at random such that:

$$1 = \sqrt{\alpha^2 + \beta^2 + \gamma^2} \qquad (9)$$

The direction cosines and the starting point coordinates serve to define the initial trajectory of the molecule. The molecule's movement is tracked along this line until it misses the solid or intersects a sphere. If it misses the solid, new direction cosines are selected and the process is repeated. If the molecule does intersect a sphere, the coordinates of the intersection point must be calculated. For sphere center (x_c, y_c, z_c) and starting point (x_s, y_s, z_s), the intersection point is given by:

$$x_i = p\alpha + x_s \qquad (10)$$
$$y_i = p\beta + y_s \qquad (11)$$
$$z_i = p\gamma + z_s \qquad (12)$$

and

$$x' = x_s - x_c \qquad (13)$$
$$y' = y_s - y_c \qquad (14)$$
$$z' = z_s - z_c \qquad (15)$$
$$p = -(x'\alpha + y'\beta + z'\gamma) - [(x'\alpha + y'\beta + z'\gamma)^2 - (x'^2 + y'^2 + z'^2 - .25)]^{.5} \qquad (16)$$

After the intersection point is calculated, a new molecular path is determined. This new trajectory is independent of the old. The coordinate system for these calculations is illustrated in Figure 3. The azimuthal angle, Φ, is randomly chosen to fit a cosine probability distibution and the rotation

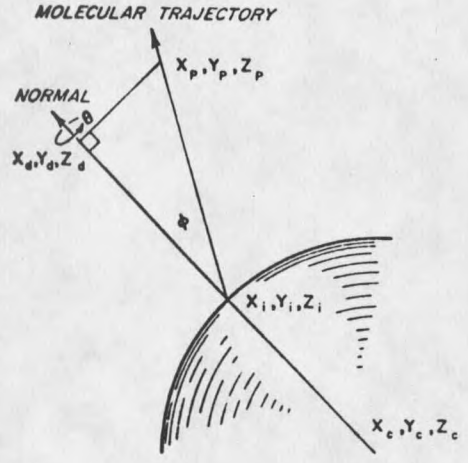

Figure 3. Calculation coordinate system.

angle, θ is chosen to fit a uniform distribution with limits of 0 and 2π. The problem is to determine the point, x_p, y_p and z_p, such that the new direction cosines may be determined. The calculation scheme is this:

1. Determine the coordinates of the point (x_d, y_d, z_d) on the normal to the surface.

$$x_d = 2x_i - x_c \quad (17)$$
$$y_d = 2y_i - y_c \quad (18)$$
$$z_d = 2z_i - z_c \quad (19)$$

2. Find normal direction numbers(a,b,c).

$$a = 1 \quad \text{if } x_c > x_i \quad (20)$$
$$a = -1 \quad \text{if } x_c < x_i \quad (21)$$
$$b = a(y_i - y_c)/(x_i - x_c) \quad (22)$$
$$c = a(z_i - z_c)/(x_i - x_c) \quad (23)$$

3. Find the distance, n, between d and p.

$$n = 2\tan(\Phi) \quad (24)$$

4. Find the coordinates of point p

$$y_p = y_d + \frac{(\theta - \pi)}{2\pi}\sqrt{\frac{n^2}{1 + b^2/a^2}} \quad (25)$$

$$z_p = [-A + \text{sign}\ (B^2 - 4\ A\ C)^{.5}]/(2A) \quad (26)$$
$$A = 1 + c^2/a^2 \quad (27)$$
$$B = -2\ [z_d A + b\ c(y_d - y_p)/a^2] \quad (28)$$
$$C = z_d\ [z_d A + 2\ b\ c(y_d - y_p)/a^2] - n^2 + (1 + b^2/a^2)(y_d - y_p)^2 \quad (29)$$
$$\text{sign} = 1 \text{ or } -1, \text{ 50\% probability.} \quad (30)$$
$$x_p = x_d + [b(y_d - y_p) + c(z_d - z_p)]/a \quad (31)$$

5. Find the new direction cosines.

$$\alpha = (x_p - x_i)/D \quad (32)$$
$$\beta = (y_p - y_i)/D \quad (33)$$
$$\gamma = (z_p - z_i)/D \quad (34)$$
$$D = \sqrt{(x_p - x_i)^2 + (y_p - y_i)^2 + (z_p - z_i)^2} \quad (35)$$

The movement of the molecule is now tracked until another collision occurs. Equations 10-35 are repeatedly applied until the molecule is reflected or transmitted. If reflected, the maximum depth of penetration is recorded. If a molecule's trajectory is such that it leaves the solid through a side, new values of θ and Φ are determined at the last intersection point. A typical simulation consists of 100 to 10,000 trials with computation times ranging from .1 to 10 hours using a VAX 11/ 750.

RESULTS AND DISCUSSION

In order to determine how many trials(ie. molecules tracked) are necessary, simulations were carried out using from 100 to 10,000 trials. Tests of a simulation are the ability of a plot of f_t versus 1/L to fit a straight line(per Eq. 8) and for the slope to be independent of the number of trials. Figure 4 represents the results of these calculations for one model solid(ϵ=.543). For all calculations, $f_t L$ was found to be constant after 10,000 trials. The deviation of both lines from straight line behavior at high 1/L values is caused by entrance effects. Our calculations are based on the slope in the region(1.2<1/L<2).

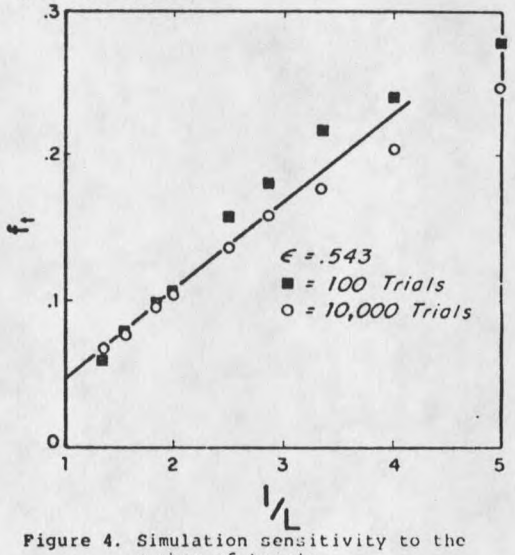

Figure 4. Simulation sensitivity to the number of trials.

As stated earlier, the effective diffusivity is determined from the slope of f_t versus 1/L using Equation 8. The effect of porosity on these plots is illustrated in Figure 5. As one would expect $f_t L$ and hence, D_e, decrease with lower porosity due to a smaller cross-sectional area and effective pore size.

Table 1 is a summary of our findings for the 5 model solids studied. As long as geometric similarity is maintained, the transport rate should be directly proportional to the sphere size. Therefore, findings are expressed in terms of d_s.

ϵ	$f_t L$	$D_e/\sqrt{T/M}$	$\bar{d}$	τ
.386	.0308	1120 d_s	.419 d_s	1.40
.438	.0353	1284 d_s	.520 d_s	1.72
.466	.0455	1655 d_s	.582 d_s	1.59
.512	.0515	1873 d_s	699 d_s	1.85
.543	.0519	1888 d_s	.792 d_s	2.21

Table 1. Simulation summary.

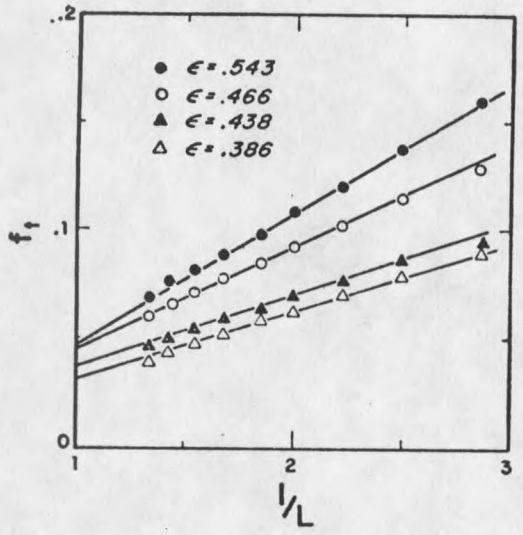

Figure 5. Variation of f_t with changing porosity.

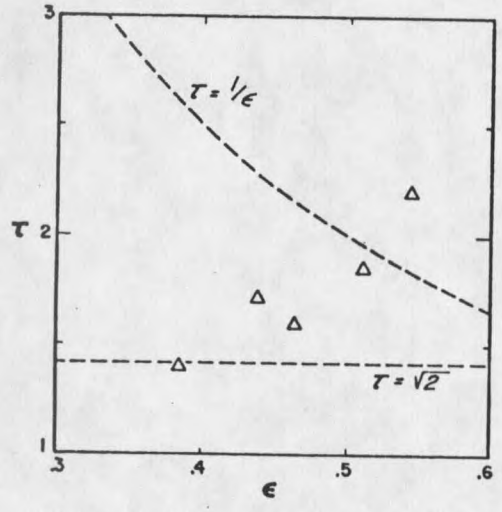

Figure 6. Effect of porosity on calculated tortuosity factors.

Figure 6 illustrates the interesting result that when the porosity is equal to its limiting value(ϵ=.37) for random packings of uniform spheres, the tortuosity factor is equal to 1.40. This value is identical to the tortuosity factor predicted from the effects of pores being, on average, 45 degrees from the direction of flow. This implies that when the "hydraulic diameter" (Equations 6 and 7) is used, no effect due to the nonideal shape of the pore is realized. This would not be true when the pore diameter is based on values determined from mercury porosimetry or sorption isotherm analysis. Also plotted in Figure 6 is the function $1/\epsilon$. In the absence of information about the value of the tortuosity factor, this function is usually used as a first approximation[5].

There appears to be no fundamental reason why the use of a "hydraulic diameter" accounts for the nonuniform pore shape when the porosity is at its limiting value. In studies of bulk diffusion in random assemblages of spheres, Hoogschagen[16] has reported values of τ between 1.4 and 1.6 but the pore diameter does not affect bulk diffusion.

ACKNOWLEDGEMENTS

Financial support for this project has been provided by the MSU Engineering Experiment Station and the Sigma Xi Research Society and is gratefully acknowledged.

REFERENCES

1. Weisz, P.B., "Zeolites-New Horizons in Catalysis," Chem. Tech., 504, (1973).

2. Knudsen, M., "Die Gesetze der Molekularstromung und der inneren Reibungsstromung der Gase durch Rohren," Annal.Physics 28, 73, (1928).

3. Smith,J.M., CHEMICAL ENGINEERING KINETICS, McGraw-Hill, (1970).

4. Wheeler, A. CATALYSIS, VOL.2, Ed. P.H. Emmett, Reinhold, (1955).

5. Satterfield, C.N. MASS TRANSFER IN HETEROGENOUS CATALYSIS, MIT PRESS, (1970).

6. Michaels, A.S., "Diffusion in a Pore of Irregular Cross Section-A Simplified Treatment," AIChEJ, 5, 273, (1959).

7. Strieder, W. and Aris, R., VARIATIONAL METHODS APPLIED TO PROBLEMS OF DIFFUSION AND REACTION, Springer-Verlag, (1973).

8. Carman, P.C., "Diffusion and Flow of Gases and Vapours through Micropores. I. Slip Flow and Molecular Streaming," Proc.Roy. Soc. A, 203, 55, (1950).

9. Evans J.W., Abbasi, M.H. and Sarin, A., "A Monte Carlo Simulation of the Diffusion of Gases in Porous Solids," J.Chem.Phys., 72, 5, 2967, (1980).

10. Abbasi M.H., Evans, J.W. and Abramson, I.S., "Diffusion of Gases in Porous Solids: Monte Carlo Simulations in the Knudsen and Ordinary Diffusion Regimes," AIChEJ, 29, 4, 617, (1983).

11. Lowell, S., INTRODUCTION TO POWDER SURFACE AREA, J. Wiley & Sons, (1979).

12. Mason, G., "A Model of the Pore Space in a Random Packing of Equal Spheres," J. Colloid Sci., 35, 279, (1971).

13. Scott, G.D., "Radial Distribution of the Random Close Packing of Equal Spheres," Nature, 194, 956, (1962).

14. Haughey, D.P. and Beveridge, G.S.G., "Structural Properties of Packed Beds-A Review," Can.J.ChE. 47, 130, (1969).

15. VAX-11 FORTRAN LANGUAGE REFERENCE MANUAL, Digital Equipment Corporation, (1982).

16. Hoogschagen, J., "Diffusion in Porous Catalysts and Adsorbents," Ind.Eng.Chem., 47, 907, (1955).

APPENDIX B

PARTITIONING OF RIGID MACROMOLECULES IN ASSEMBLAGES OF SPHERES

The equilibrium partitioning of rigid, spherical macromolecules between the pore volume in a random packing of solid spheres and the bulk liquid phase is considered. The effect of changing λ (molecule size/pore size) on the partition coefficient has been determined and is compared to theoretical values for various pores of well-defined shape.

INTRODUCTION

The phenomena of macromolecule partitioning occurs in a number of engineering applications such as membrane transport and catalysis as well as several macromolecule separation schemes. Macromolecules are excluded from a portion of the porous media's void volume if the molecules size is not negligible with respect to the pore diameter. This partitioning effect and its relation to restricted diffusion has been the subject of numerous studies for porous solids of well defined pore shapes. However, many porous materials are not adequately described by pores of a single, well defined geometry. It is the intention of this work to investigate this size exclusion effect for spherical, non-interacting macromolecules in a random pore system. What could be considered to be the opposite extreme from the classic well-defined cylindrical pore is the pore network surrounding an assemblage of solid spheres which are randomly packed. This pore model is more representative for the many porous materials manufactured from the agglomeration of very fine powders such as silica or alumina sols.

The magnitude of this geometric exclusion effect for solid, non-interacting spheres in cylindrical pores is given by Ferry [1]. That expression may be generalized for other well defined pore shapes using geometric arguments to obtain:

$$K_p(\lambda) = (1-\lambda)^n \qquad (1)$$

where: n = 1 for flat plates.
n = 2 for cylinders.
n = 3 for spherical cavities and cones.
K_p = pore concentration/bulk concentration.

Casassa and Tagami[2] have developed analogous expressions for rigid linear polymer chains in well-defined pores:

$$K_p(\lambda) = 2\,n \sum_{m=1}^{\infty} \exp(-\rho_m^2\lambda^2)/\,\rho_m^2 \qquad (2)$$

where: $\rho_m = (2m+1)\pi/2$ for n=1.
ρ_m = zero's of $J_0(\rho_m)$ for n=2.
λ = root mean square radius of gyration/r.

Giddings and co-workers[3] present a general expression for the equilibrium partition coefficent by considering the loss in configurational entropy of various shape particles in a variety of pore shapes. For rigid molecules of any shape in a isotropic network of random planes, they obtain:

$$K_p(\lambda) = \exp(-L'/2r) \qquad (3)$$

where: L' = mean length of projection.

Although a random pore network was considered, the approach used is intractable for more realistic pore networks such as a random packing of spheres.

ANALYSIS

A method of theoretically generating a random packing of spheres of a single diameter with properties(ie. coordination

#, sphere spacing) similar to those experimentally observed by Scott[4] has been described by Mason[5]. The basis of this technique is to fix the coordinates of each solid sphere in space. Pores are thus, the void volume within this network of spheres. The shape and volume of a particular pore is fixed by joining the centers of four neighboring spheres together to form a tetrahedron. Since the four spheres are not necessarily touching, the distribution of distances between the sphere centers(ie. tetrahedron edge lengths) is the only remaining information necessary to fix the entire pore structure. The edge length distribution given by Mason[6] is:

$$N = 7.5 + 15.62\,(x-1) \qquad (4)$$

where N = # of centers within distance x.
x = sphere center distance in sphere diameters.

This distribution predicts that 7.5 spheres will touch a given reference sphere(ie. coordination # =7.5) and a total of 13.75 sphere centers are within the range of 1 to 1.4 diameters.

Following Mason, Equation 4 was used in conjunction with a uniform random number generator to determine the sphere center distances(ie. edge lengths). A total of 10,000 random tetrahedra (60,000 edge lengths) have been calculated and analyzed using a VAX 11/750 computer. The volume of each tetrahedron is calculated as well as the solid angle for each of the four vertices. Summing all four solid angles, the tetrahedron volume occupied by solids is determined. The porosity corresponding to each of these tetrahedon and the porosity distribution is calculated. Our calculated value of

39% for the average porosity agrees fairly well with the experimental value of 37% reported by Scott[4].

In order to obtain the equilibrium partition coefficient, the reduction in accessable pore volume for each of the random tetrahedron as a function of λ must be calculated. The partition coefficient for solid, non-interacting spheres may be defined as:

$$K_p(\lambda) = \epsilon(\lambda)/\epsilon(\lambda=0) \qquad (5)$$

The reduction of porosity for a particular tetrahedron as a function of λ is calculated using the solid angles for each vertex combined with an effective solid sphere radius which is increased by the radius of the macromolecule. K_p for the entire pore network is obtained from a weighted average of ϵ for all 10,000 tetrahedra and Eq. 5.

RESULTS

The average reduction in accessable pore volume for 10,000 tetrahedra as a function of the size parameter, λ, is plotted in Figure 1. In addition, the partition coefficient given by Equation 1 for slab, cylindrical and spherical pores(ie. n=1,2,3) is presented. One major question for pores in assemblages of spheres is how to relate the pore radius to the size of the solid spheres which form the network. For pores of well defined geometery, the characteristic pore size is obvious and may be determined from experimental measurements. Common methods of characterizing the pore size are to either take twice the pore volume to surface area ratio or measure

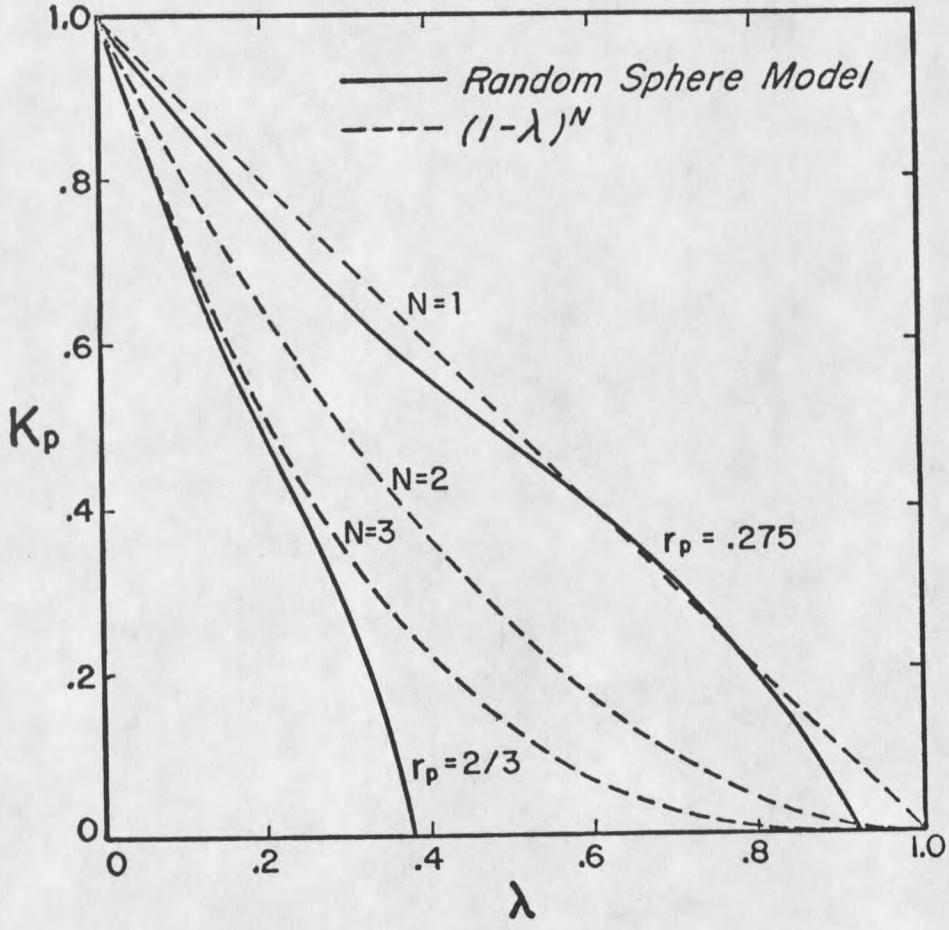

Figure 1 Variation of equilibrium partition coefficient with λ. Random pore model.

the pore size directly via mercury porosimetry or adsorption isotherm analysis. Only for cylindrical pores will these two methods be in complete agreement. Taking twice the ratio of volume to surface area, implies that the pore radius is 2/3 of the solid sphere radius(r_p=2/3). However, if we assume that the pore size measured by mercury porosimetry is equal to the average size of a particle that would fit between three adjacent solid spheres, the average pore radius is .275 times the sphere radius. Therefore, we have calculated K_p using values of λ determined using both of these definitions for relating λ to the size of the solid spheres.

If we relate the pore radius to the solid sphere radius using twice the ratio of pore volume to surface area(r_p=2/3), the K_p- λ relationship is very similar to Equation 1 with n=3 for λ <.25. However, at larger λ values, our random pore model predicts a rapid decrease in K_p. In this region, the molecule size is such that macromolecules are excluded from entering certain tetrahedra. The largest possible tetrahedron face has three edge lengths of 1.4(see Eq. 5). This corresponds to complete molecule exclusion at λ =.38 when r_p=2/3. For r_p=.275, our calculated K_p relationship varies between the predictions of Eq. 1 with n=1 and n=2. We should note that this finding is similar to experimental results reported by several investigators using catalyst supports.

Results for equilibrium partitioning in regular packing configurations of solid spheres are presented in Figure 2. The change in K_p as a function of λ has been calculated for

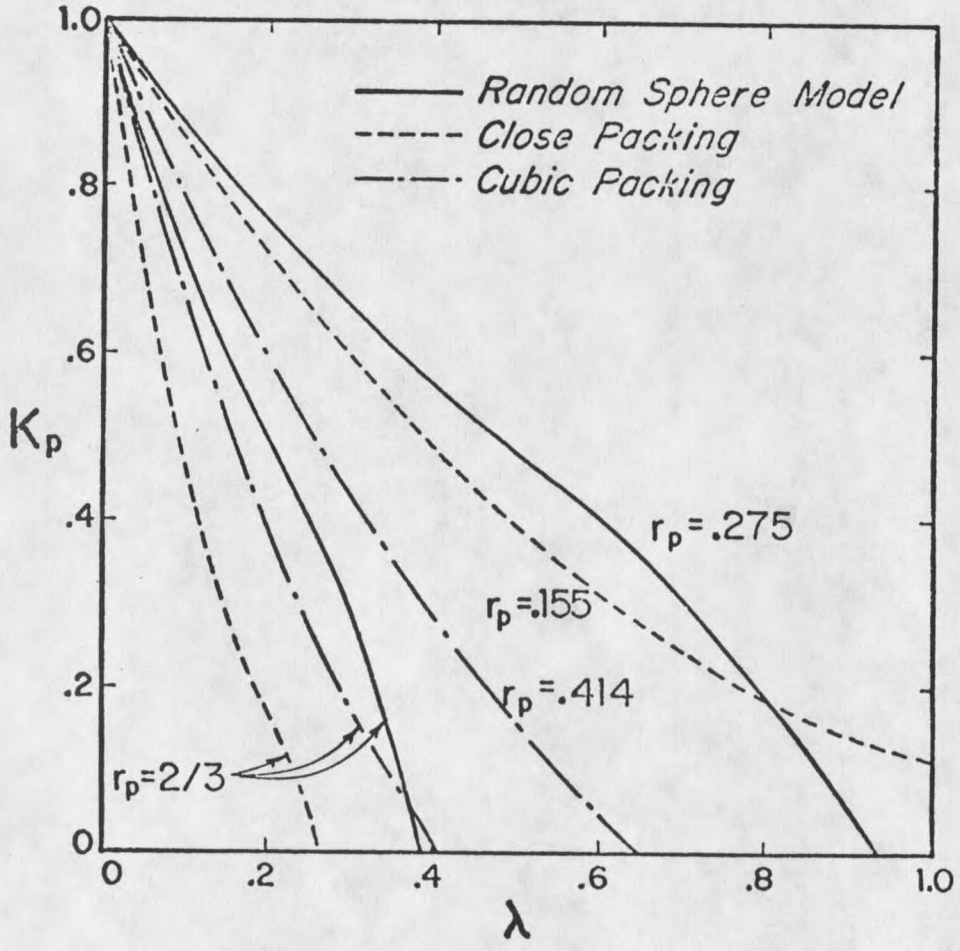

Figure 2 Variation of equilibrium partition coefficient with λ. Effect of packing configuration.

both cubic and close-packed hexagonal packing configurations. Since these pore models have a larger surface area to pore volume ratio, the rapid decrease of K_p with λ is expected when basing our λ on that ratio. If we use the average particle size which will fit between three adjacent solid spheres to characterize the pore radius, a much slower decrease of K_p with λ is found.

It appears that this is the first time that the importance of HOW the pore radius is measured has been discussed with respect to macromolecule partitioning. As evidenced by Figure 1, how λ is calculated has a major effect on the value of K_p. It is quite possible that this is why that there exists so little agreement between various experimental and theoretical studies of partitioning as reported in the literature. Only when track-etched membranes(ie. ideal cylindrical pores) are used are findings generally in agreement.

NOMENCLATURE

K_p = Equilibrium partition coefficient.

L' = Mean length of projection.

n = Pore geometry factor.

N = Number of sphere centers within distance x.

r = Pore radius.

r_p = Pore radius/solid sphere radius.

x = Distance between two solid sphere centers.

ϵ = Porosity.

λ = Molecule radius/pore radius.

ρ = Eigenvalues defined by Eq. 2.

REFERENCES AND NOTES

1. Ferry,J.D.,"Statistical Evaluation of Sieve Constants in Ultrafiltration", J.Gen.Physiol., 20, 95, (1936).
2. Casassa,E.F. and Y. Tagami,"An Equilibrium Theory for Exclusion Chromatography of Branched and Linear Chains",Macromol., 2, 14, (1969).
3. Giddings,J.C., E.Kucera, C.P.Russell and M.N.Myers, "Statistical Theory for the Equilibrium Distribution of Rigid Molecules in Inert Porous Networks. Exclusion Chromatography",J.Phys.Chem., 72, 4397, (1968).
4. Scott, G.D.,"Packing of Equal Spheres", Nature, 188, 910, (1960).
5. Mason, G.,"A Model of the Pore Space in a Random Packing of Equal Spheres", J.Colloid Sci., 35, 279, (1971).
6. Mason, G.,"Radial Distribution Functions from Small Packings of Spheres", Nature, 217, 733, (1968).